Spectroelectrochemistry of self-assembled monolayers of 2- and 4-mercaptopyridines

von der Fakultät für Naturwissenschaften der Technischen Universität Chemnitz
genehmigte Dissertation zur Erlangung des akademichen Grades

doctor rerum naturalium

(Dr. rer. nat.)

Vorgelegt von

M.Sc. Nazly Abdel Salam Ibrahim Hassan

geboren am 12.03.1968 in Alexandria (Egypt)

eingereicht am 25.01.2007

Gutachter: Prof. Dr. Rudolf Holze

Dr. Alexander Auer

Dr. Andreas Bund

Tag der Verteidigung: 20.06.2007

Bibliographische Beschreibung und Referat

N. Hassan

Spectroelectrochemistry of self-assembled monolayers of 2- and 4-mercaptopyridines

Die Elektrochemie und die Spektroelektrochemie von selbst-organisiererten Monoschichten (self-assembled monolayers, SAMs) gebildet aus 2-Mercaptopyridin (2MP) und 4-Mercaptopyridin (4MP) wurden an polykristallinen Goldelektroden in wässrigen Elektrolytlösungen untersucht. Folgende Untersuchungsmethoden wurden angewandt: zyklische Voltammetrie, elektrochemische Impedanzmessungen (EIM) und oberflächenverstärkte Raman Streuung (surface-enhanced Raman scattering, SERS).

Die elektrochemischen Untersuchungen von 2MP und 4MP in wässriger saurer Lösung (0.5 **M** H_2SO_4) zeigten, dass 2MP stärker adsorbiert wird als 4MP aufgrund der Bildung eines S-Au-N-Chelates, wobei die S-Au-Interaktionen bei 4MP stärker sind. Die Bildung eines Chelates im Falle von 2MP verringert die Wahrscheinlichkeit der Bildung eines Dimers. In sauren Lösungen wird das N-Atom von 2MP protoniert, was zu einer schwächeren Bindung von 2MP-Molekülen zur Substratoberfläche führt. Die Ergebnisse der SERS-Untersuchungen stimmen mit den Resultaten aus der zyklischen Voltammetrie überein. Man erhält eine Au-S-Streckschwingungsbande für 2MP zwischen 225 bis 250 cm^{-1} bei Abscheidung aus wässriger oder saurer Lösung und für 4MP bei ca. 263 cm^{-1} in beiden Lösungen. Die SERS-Experimente ergaben eine senkrechte Orientierung zur Goldoberfläche sowohl für 2MP als auch für 4MP. Die Thion-Thiol-Tautomerie von 2-Mercaptopyridinen wurde ebenfalls in Betracht gezogen.

Die Unter- und Überpotentialabscheidung von Kupfer auf einer polykristallinen Goldelektrode in wässriger 0.1 **M** Schwefelsäure in An- und Abwesenheit von SAMs von 2- und 4-Mercaptopyridin wurde mit zyklischer Voltammetrie untersucht. Es zeigte sich, daß bei Vorhandensein der SAMs die Elektrodeposition von Kupfer verhindert wird, was auf starke Wechselwirkungskräfte zwischen dem Adsorbat (MP) und der Goldoberfläche zurückzuführen ist. 2MP zeigt eine grössere Inhibierung, was höchstwahrscheinlich auf die Bildung der Chelatstruktur zurückzuführen ist. Es wurden ebenso Untersuchungen zum Einfluss von 2MP und 4MP auf die abgeschiedene Kupfermonolage auf der Goldelektrode durchgeführt. Es zeigte sich, daß die Kupfermonolage teilweise durch 2MP oder 4MP ersetzt wird.

Die Elektronenaustauschgeschwindigkeit für das Fe^{2+}/Fe^{3+}-Redoxsystem in An- und Abwesenheit von 2MP- oder 4MP-Monolagen wurde mit zyklischer Voltammetrie und elektrochemischen Impedanzmessungen (EIM) untersucht. Es stellte sich heraus, dass der Elektronenaustausch höchstwahrscheinlich über Defektstellen in der Monolage (Pinholes) erfolgt. In einer wässrigen Lösung verringert 4MP den Elektronenaustausch stärker als 2MP. Da die Packungsdichte bei 4MP größer ist als bei 2MP ist wahrscheinlich auch die Zahl der Pinholes geringer in der 4MP-Monolage. In saurer Lösung liegen die N-Atome protoniert vor. Man kann davon ausgehen, dass in saurer Lösung zwei Prozesse gleichzeitig ablaufen, die für den Elektronenaustausch entscheidend sind. Erstens kommt es zu einer Abstoßung zwischen der positiv geladenen Monolage und den positiv geladenen Redoxionen. Und zweitens erfolgt eine Abstoßung zwischen den positiv geladenen Molekülen der SAMs, was zu einer geringeren Packungsdichte führt. Der Ladungsaustausch wird dominiert durch den zweiten Effekt.

Mit Hilfe von EIM wurden die Elektronenaustauschgeschwindigkeit und der Bedeckungsgrad bestimmt.

Die korrosionshemmende Wirkung von 2MP und 4MP auf Stahl in 3.5 % wässriger NaCl-Lösung wurde mit Hilfe der EIM untersucht. 2MP zeigte eine grössere Hemmung als 4MP.

Stichwörter: Spektroelektrochemie, Elektrochemie, selbst-organisierende Monoschichten, 2- und 4-Mercaptopyridin, Zyklische Voltmmetrie, EIM, Elektronenaustausch, SERS, Korrosionshemmung

Abstract

N. Hassan

Spectroelectrochemistry of self-assembled monolayers of 2- and 4-mercaptopyridines

The electrochemistry and spectroelectrochemistry of the self-assembled monolayers (SAMs) prepared of 2-mercaptopyridine (2MP) and 4-mercaptopyridine (4MP) dissolved either in water or 0.1 **M** H_2SO_4 have been investigated at polycrystalline gold electrodes in aqueous electrolyte solutions using cyclic voltammetry, electrochemical impedance measurements (EIM) and surface enhanced Raman spectroscopy (SERS).

Electrochemical studies of 2MP and 4MP monolayers in aqueous acidic solution (0.5 **M** H_2SO_4) suggest that 2MP is adsorbed more strongly than 4MP due to the formation of S-Au-N chelate. However, the S-Au bond was found to be stronger in 4MP as compared with 2MP. The formation of the chelate in case of 2MP diminishes the probability of dimer formation. In the acidic solvent, the N-atom of 2MP molecule will be protonated leading to a weaker interaction of 2MP molecules with the substrate surface. The SERS results are in good agreement with the cyclic voltammetry results. The Au-S stretching band was obtained in the region from 215 to 245 cm^{-1} for 2MP deposited from water and acidic solvent and around 263 cm^{-1} for 4MP in both solvents. The SERS measurements showed also a perpendicular orientation of both 2MP and 4MP on the gold surface. In explaining the SERS results, the thione-thiol tautomerisations of the mercaptopyridines were also taken into consideration.

The under- and overpotential deposition of copper on a polycrystalline gold electrode in aqueous 0.1 **M** sulfuric acid in the presence and in the absence of SAMs of 2- and 4-mercaptopyridine has been studied using cyclic voltammetry. In general, the presence of these SAMs has been found to inhibit the electrodeposition process of copper, suggesting very strong interactions between these adsorbates and the Au surface. 2MP shows a higher degree of inhibition, which is due to a stronger interaction probably due to the formation of the chelate structure. Studies have also been made of the influence of mercaptopyridines SAMs on the copper monolayer electrodeposited on the gold surface. The copper adlayer was found to be partially displaced by 2MP and 4MP monolayers.

The rate of electron transfer for the $Fe^{3+/2+}$ redox system on the gold electrode has been probed in the absence and presence of 2MP and 4MP monolayers by cyclic voltammetry and electrochemical impedance measurements (EIM). The charge transfer process was suggested to occur through the defects (pinholes) in the monolayer. In case of aqueous solvent 4MP decreases the electron transfer reaction stronger than 2MP. Since the packing density for 4MP is higher than that of 2MP the number of pinholes might be lower in 4MP monolayer. In acidic solvent the N-atoms of the mercaptopyridines will be protonated. It is proposed that two effects, which exist at the same time, are responsible for the electron transfer process in acidic solution. First, there will be a repulsive interaction between the positively charged monolayer and the positively charged redox probe. Second, there is a repulsion among the positively charged monolayer molecules that results in a less compact monolayer. The charge transfer is dominated due to the latter effect. With the EIM the rate of electron transfer and the surface coverage were determined.

2MP and 4MP were examined as steel corrosion inhibitors in 3.5% aqueous NaCl solution using EIM. 2MP shows higher inhibition efficiency than 4MP.

Keywords: Spectroelectrochemistry, Electrochemistry, Self-assembled monolayers, 2- and 4-mercaptopyridine, Cyclic voltammetry, EIM, Electron transfer, SERS, Corrosion inhibition.

Die vorliegende Arbeit wurde in der Zeit von Januar 2002 bis Dezember 2005 unter Leitung von Prof. Dr. Rudolf Holze am Lehrstuhl für Physikalische Chemie/Elektrochemie der Technischen Universität Chemnitz durchgeführt.

Acknowledgement

First and foremost I offer my thanks, obedience, and gratitude to God from whom I received guide and inspiration.

I must extend my deep gratitude to Prof. Dr. Rudolf Holze for giving me the chance to work in his working group and for his guidance during this work. The financial support of Chemnitz University of Technology is also acknowledged.

I would like to express my deepest appreciation to Dr. Abdel Aziz Jbarah, Mrs. Susanne Vogel and Mr Fadi Alakhras for their help, friendship and encouragement.

I'm very grateful to the former and current members of the electrochemistry group for all what I have learnt from them. I show gratitude to Mrs. Salma Bilal and Dr. Hung Van Hoang for their friendship, assistance and care. I thank Dr. Subrahmanya Shreepathi and Mr. Anwar-ul-Haq Shah for their help.

To my friends (near and far), I thank you for your unchanged friendship. Special admiration should be directed to Mrs. Amal King Kordi and her husband Mr. Abdalsalam Absi for being always around in both nice and hard moments, and also to their lovely child "Aia" since she was a nice smile in my days. I wish every one of them all the best in their life and I wish Mrs. King Kordi a great success in her PhD.

I'm deeply grateful to Mrs. Carolin Schubert for her friendship and care. Her kindness and consideration will be always remembered. I wish her all the best with her husband and her little daughter. I'm also indebted to Mr. Ahmed's family; they kindly considered me as a member of their family.

My appreciation to all of them. I wish to thank Mr. Paul Friedrich for taking care of my computer and solve all the problems I got with it in the critical times. Also I thank him for his friendship.

Finally, great thanks are owed to my family in Egypt for their support, care and love. Special thanks are extended to my sister Hala Hassan, her calls were always enough to make me very strong, and also to my uncles Mohamed Nassar and Abdel-Razeq Nassar, their concern and love are the backbone to my success.

My parents, the ones that I will be proud of forever, their praying were always protecting me. I have learnt a lot from them, like being optimistic even in very difficult times. The words are unable to describe what they've done for me all my life. I owe any progress from the first moment in my life to them.

Again, I thank everyone gave and still giving me support, advice and criticism. I deeply appreciate everyone who has played a role in supporting my effort.

Dedication

Dedicated to my parents

To my brother and my sisters

To the soul of my uncle / Sabry Nassar

To all members of my family

Yes, anything can be achieved through the will of

God

Nazly

- *Table of Contents* -

List of Abbreviations

Fig.	Figure
UHV	Ultra high vacuum
LB	Langmuir-Blodgett
SAM	Self-assembled monolayer
SAMs	Self-assembled monolayers
2-D	two dimensional
2MP	2-mercaptopyridine
4MP	4-mercaptopyridine
MPs	Mercaptopyridines
ac	alternative current
CV	Cyclic voltammogram
CVs	Cyclic voltammograms
MSE	Hg/Hg_2SO_4 electrode in 0.1 **M** K_2SO_4
RHE	Reversible hydrogen electrode
SCE	Saturated calomel electrode
Au/2MP	Au electrode pretreated with 2MP
Au/4MP	Au electrode pretreated with 4MP
vs	versus
dE/dt	Scan rate
eq.	Equation
UPD	Underpotential deposition
OPD	Overpotential deposition
EIM	Electrochemical impedance measurement
ΔE_p	Peak-to-peak separation or peak potential separation
E_{pc}	Cathodic peak potential
E_{pa}	Anodic peak potential
O	Oxidant
R	Reductant
I_p	Peak current
I_{pa}	Anodic peak current
I_{pc}	Cathodic peak current

E_f	Formal potential
E_m	Midpoint potential
ET	Electron transfer
CT	Charge transfer
D	Diffusion coefficient
D_{eff}	Effective diffusion coefficient
Z	Impedance
Z'	Real part of impedance
Z''	Imaginary part of impedance
CPE	Constant phase element
Q	Magnitude of the constant phase element
Z_{CPE}	Impedance of the constant phase element
R_s	Solution resistance
R_{ct}	Charge transfer resistance
C_{dl}	Double layer capacitance
W	Warburg impedance
k	Rate constant
θ	Surface coverage
R_p	Polarization resistance
SERS	Surface enhanced Raman spectroscopy
SER spectra	Surface enhanced Raman spectra
E_{MSE}	Potential *vs* the MSE electrode
E_{RHE}	Potential *vs* the RHE electrode
#	Number
ν	Stretching mode
β	Bending mode
$\beta_{i.p.}$	In-plane bending mode
δ	In-plane deformation mode
γ	Out-of-plane deformation mode
n.a.	Not assigned

-Introduction-

1 Introduction

Interfacial reactions are becoming an increasingly important subject for studies. The ability to control the chemical and structural properties of surfaces is essential for the progress in catalysis, electronics, chemical sensing and many other applications. In parallel, understanding the rules that govern surface reactions provides very important information for fundamental studies in chemistry. These considerations and the availability of numerous analytical techniques to detect the chemical changes in thin films have made studies of interfacial reactions an important area of modern science.

1.1 Organic thin films

Organic thin films have attracted a considerable interest over the last years, although the subject has fairly old roots. More than 200 years ago, Franklin [1] observed the calming influence of oil on water surfaces. In the 19th century, Pockels [2-5] prepared monolayers at the air-water interface, followed by the works of Rayleigh [6], Hardy [7], Devaux [8] and others. Later monolayers of amphiphilic molecules on the water surface were named after Langmuir [9,10].

The deposition of long-chain carboxylic acids was studied for the first time by Blodgett [11,12] on solid substrates. Around that time, amphiphilic monolayers were already used to control the wetting behaviour of metal condenser plates in steam engines [13-15]. In addition, researches focusing on self-assembled monolayers were performed later by Zisman [16], Blackman and Dewar [17].

Interest in the properties of thin organic materials, especially coherently organized assemblies, has grown enormously in recent years, primarily due to the ease of fabrication, characterization and manipulation. Organic thin films usually display optical, electrical, optoelectronic, mechanical, chemical and other properties used in many applications, which are not accessible with inorganic materials.

These films can be prepared by several methods. <u>Fig.1</u> shows schematically the most common methods used for preparing organic thin films:
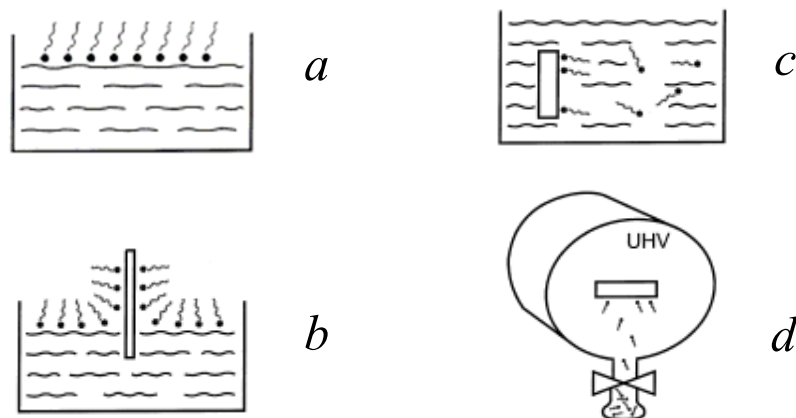
Fig. 1   Most common methods used for preparing organic thin films as reported in reference [18]. Langmuir films (a), Langmuir-Blodgett films (b), Self-assembled monolayers grown from solution (c) and Self-assembled monolayers grown from ultra high vacuum (d) [18].

1. Langmuir films consist of amphiphilic molecules spread on a liquid surface like water. The hydrophilic head group has an affinity to the water while the hydro-phobic end group sticks out on the other side [19,20].

2. Langmuir-Blodgett (LB) films are prepared by transferring Langmuir films onto a solid substrate [21]. The head group is hydrophilic while the tail group is hydrophobic, so that the direction of the molecules is achieved prior to the transfer step. Multilayers are prepared by repeated (periodic) dipping of the substrate in appropriate solutions. Interest in LB layers continues unabated to this day due to possible technical applications in sensors, corrosion inhibition, lubrication and photoresists [22-25].

3. Self-assembled monolayers grown from solution or from the gas-phase represent a further class of organic thin films. The significant feature is the chemisorption (or, generally, strong interaction) of the head-group with a specific affinity to the sub-strate. Self-assembled monolayers grown from solution will be discussed in more details in next sections.

The phenomenon of self-assembly has been recognized for nearly 60 years[16], nevertheless, it has not enjoyed the popularity of Langmuir-Blodgett (LB) layers until more recently. In contrast to Langmuir-Blodgett films, self-assembled monolayers of organic compounds can be obtained simply by chemical adsorption from aqueous or organic solutions. Compared with the LB technique, the self-assembling method has more advantages [26]: (i) the interactions between the layers are very strong like chemical bonds, metal complexations or electrostatic interactions; (ii) there is less limitation on the types of the molecular building blocks that can be used; (iii) it does not need a specific experimental apparatus. Therefore, the self-assembling method seems to be simpler and more flexible, and for these reasons appears to be very attractive.

1.2   Self-assembled monolayers

In general sense, self-assembled monolayers (SAMs) can be defined as well-ordered and oriented molecular films, which are formed spontaneously, upon immersion of a substrate (solid surface) into a solution containing an active surfactant molecule. These molecules organize themselves in a two-dimensional (2-D) arrangement on the surface of the substrate.

The field of SAMs has witnessed incredible development and depth of characterization over the past 20 years. On the other hand, it is interesting to comment on the humble beginning and on important milestones. The field really began much earlier than is now recognized [27]. In 1946, Zisman [16] published the preparation of a monomolecular layer by adsorption (self-assembly) of a surfactant onto a clean metal surface. In 1983, Nuzzo and Allara [28] showed that SAMs of alkanethiolates on gold can be prepared by adsorption of di-*n*-alkyl disulfides from dilute solutions. This work sparked attention in exploring SAM systems based on sulfur-metal interactions. Soon afterwards, it was revealed that other organosulfur compounds such as alkanethiols and alkyl sulfides can be also assembled on the surfaces of metals such as gold, silver and copper to afford SAMs [29-31]. Many self-assembly systems have been investigated since this time but the most studied SAMs to date are alkanethiolates on gold [27].

Successful self-assembling requires a relatively strong bond between the substrate and an atom or moiety in the molecule and an additional lateral interaction between the molecules in the monolayer. The degree of order in monolayers depends upon many factors, including geometric considerations, electrostatic and dipole-dipole interactions within the monolayers and affinity of the head group of the surfactant to the surface. The simplicity and flexibility of the self-assembly process provides an opportune method for varying the properties of the metal as an electrode [32,33].

SAMs must fulfil at least three requirements: (1) to be strongly attached to the substrate, therefore the surfaces will resist environmental chemical and physical effects, (2) to be homogeneous and closely packed, accordingly the model surfaces will have a given and well-defined composition and (3) to allow different functional groups to be attached to the surface, thus offering a powerful way to develop systems that have several applications [34].

1.3   Organosulfur compounds

Sulfur compounds have a strong affinity to transition metal surfaces [35-39]. Organosulfur compounds coordinate very strongly to the surface of the metal. The number of reported surface-active organosulfur compounds that form monolayers on metal surfaces has increased in recent years.

1.3.1 Thiols

Thiols are organic compounds in which a S-atom is bonded to a carbon atom in the molecule. Their chemical structure is close to alcohols except that sulfur is substituted for the oxygen in the hydroxyl group. Thiols are also known by the term "mercaptan".

Thiol monolayers can be prepared by treatment of a gold surface under ambient conditions with a dilute solution of the thiol (< 1 **mM**). One of the important properties of such systems is that they give the possibility of controlling the molecular con-

struction at the electrode-solution interface. Thiols are very appropriate for such studies because of simplicity of preparation and the relatively large potential window within which such electrodes can operate [40].

Aromatic thiols have promising features in the preparation of thiol monolayers due to several reasons. First, aromatic thiols are highly anisotropic and the intermolecular interactions are stronger than those between the *n*-alkanethiols, which may lead to different molecular packing structures. Second, electrons are more delocalized in the aromatic rings than in the alkane chains, as a result the electrical conductance through aromatic thiols is higher. Finally, various functional groups can be attached to the opposite molecular end, which have been used to modify the electrode surface properties. In 1988 Hubbard [41] carried out the first experiment on the molecular packing structure of aromatic thiols on metal surface. Monolayers of thiols, which contain aromatic [42-48], or heterocyclic groups [49-57] have been less intensively investigated. These systems, especially when containing a pyridine end group, are used to immobilize proteins on metal surfaces [58-60].

1.3.2   Mercaptopyridines

Pyridine is a simple heterocyclic aromatic molecule with the formula C_5H_5N. Pyridine is structurally similar to benzene, with a single nitrogen atom substituted in the six-member aromatic ring for one of the carbons and one of the hydrogen atoms.

Mercaptopyridines are thiol compounds that contain both N- and S- atoms in the molecule. Mercaptopyridines can be easily adsorbed on the surface of the metal. Up to date, most of the investigations suggest that mercaptopyridines bound to the surface mainly through S-atom after cleavage of the S-H bond and formation of a metal-S bond [49,54,61-67]. However, it has been suggested also that mercaptopyridines might bind to the gold surface through its N-atom [68]. Mercaptopyridines form stable SAMs on the metallic surface, which are suitable for many applications. In the present work, 2-mercaptopyridine (2MP) and 4-mercaptopyridine (4MP) were used (Fig. 2).

Fig. 2   Structures of 2-mercaptopyridine and 4-mercaptopyridine.

1.4   Self-assembled monolayers of thiols on gold electrodes

One of the most widely used systems in the molecular self-assembling method is the chemisorption of sulfur derivatives (e.g. thiols, disulfides) on gold surfaces [69-71], due to the thermodynamically favorable formation of the gold-sulfur bond. The stability of the bond over a wide range of applied potential makes this system suitable for electrochemical purposes [72].

Efforts to accomplish the most blocking or most highly oriented monolayer on a gold substrate have led to the consideration of several factors in the self-assembly process such as substrate morphology, cleaning, thiol purity, kind of adsorbate, nature and concentration of deposition solvent, temperature, deposition time, the chain length of the thiol used and any "annealing" steps performed during or after the deposition step [73]. Unfortunately there are no definite formulas for achieving the "perfect" monolayer.

The monolayers of the organosulfur compounds on gold have superlative prop-erties combined with high structural order, flexibility in the structure of functional groups exposed at the solid-vapor or solid-liquid interface and ease of preparation and analysis. The convenience of thiols adsorbed on gold as a monolayer system is based on three considerations. First, gold is a relatively inert metal that does not form a sta-ble oxide surface [74] and it resists atmospheric contamination. Second, gold has a strong specific interaction with sulfur [75] that allows the formation of monolayers in the presence of many other functional groups [31]. Third, long-chain alkanethiols or

thiols with fused aromatic rings form a compact and impervious monolayer on gold [76].

The presence of an aromatic ring in a thiol molecule can enhance the binding between Au and the thiol, which consequently results in the formation of compact and impermeable SAMs. The behaviour of SAMs formed from thiol containing π-electron-rich aromatic substituents may prove interesting properties. In particular, aromatic thiol SAMs have received attention due to their high electronic conductivity and nonlinear optical properties [77].

The first advantage of self-assembled monolayers based on thiols is the simplicity with which SAMs are formed when gold and other metals are exposed to thiols. Normally it needs between seconds to minutes for the deposition of monolayer on the metal surface. The self-assembly method neither does require anaerobic or anhydrous conditions nor vacuum. Self-assembly is relatively insensible to the choice of solvent. While organic-free metal surfaces are desirable, the high affinity of the sulfur towards the metal enables the assembling layer to displace more weakly adsorbed impurities. Curvature of the metal surface is not a factor; substrates can range from macroscopic to submicroscopic dimensions and from smooth to highly porous surface.

A second advantage arises from the affinity of the sulfur to the metal and the strength of the bond formed. SAMs survive prolonged exposure to vacuum. It is possible to have a wide range of functional groups in the adsorbing molecule without disordering the self-assembly process or destabilizing the SAM. Considering just the family of substituted alkanethiols, the terminal substituent can be an alkane (linear, branched, perfluorinated, perdeuterated), alkene, alkyne, aromatic, halide, ether, alcohol, aldehyde, carboxylic acid, amide, ester, amine or nitrile. The "body" of the molecule can contain, for example, heteroatoms, aromatic groups, conjugated unsaturated links and other rigid rod structures, sulfones and amides.

1.5   Preparation of self-assembled monolayers

Thiol-based SAMs have previously been prepared by two methods [78]: growth from solution, which is the method used in this work, or growth from the gas phase.

In both cases, the highest possible purity of both the adsorbates and the substrates is preferred.

Growth from solution

Gold is the most popular substrate for thiol SAMs. Outstanding to its noble character, gold substrates can be handled in air without the formation of an oxide surface layer, and can resist harsh chemical treatments, which remove organic contaminants. The purity of the gold surface appears to be more important than its smoothness. Cleaning and etching steps are often part of the deposition protocol. Electrochemical cycling into the oxide formation region in dilute acid acts both as a cleaning and an annealing process; the resulting voltammogram provides an assay of the cleanliness of the gold. Alternatively, organic contaminants can be removed via exposure of the gold to a powerful oxidant. Popular oxidants include "piranha" solution (a 1:3 mixture of 30 % hydrogen peroxide and concentrated sulfuric acid at ca. 100 °C).
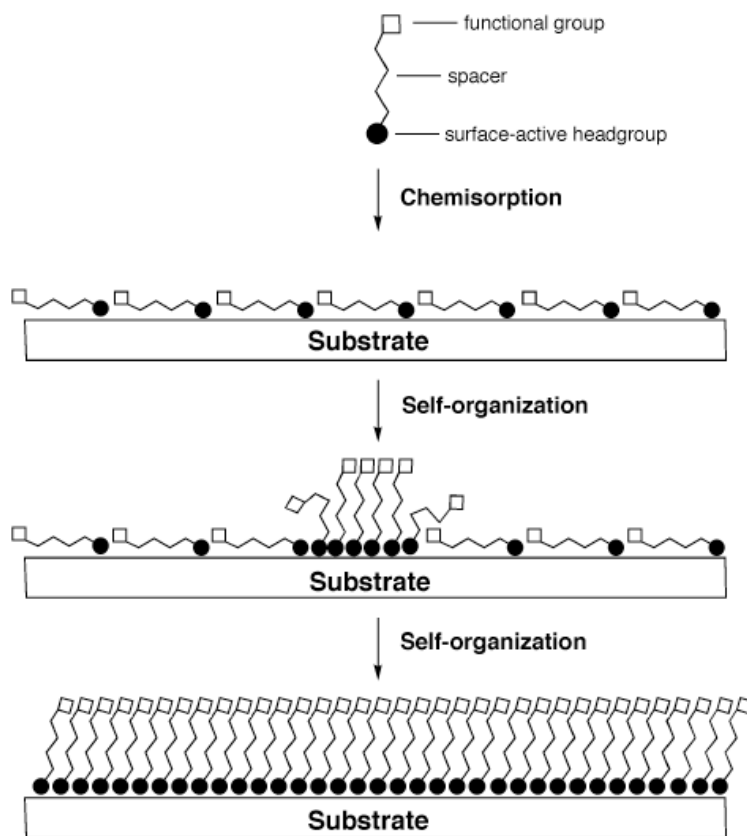
Fig. 3 Formation mechanism of the self-assembled monolayers [79].

A dilute solution of thiol (1 **μM** to 1 **mM**) dissolved in an appropriate solvent is prepared. The clean substrate is then immersed into the thiol-containing solution at room temperature, after that the monolayer-coated substrate is removed from the solution and rinsed with the solvent, which is typically the same as that used to generate the film to remove any adsorbate molecules that might be physisorbed to the surface of the monolayer. Usually any solvent capable of dissolving the molecule is suitable.

The formation mechanism of the self-assembled monolayers is displayed in (Fig. 3). Initially the thiol molecules adsorb horizontally onto the metal substrate. Afterwards, the molecules lift up to form the vertically oriented layer. This is the most common approach for depositing the SAM.

Growth from the gas phase

In this technique, the experiments are typically carried out in an ultra high vacuum (UHV) chamber. Adsorbate molecules are usually placed in a container that is connected to the chamber through a dosage valve, which is used to control the flow of adsorbate vapor into the chamber. The container may require warming to introduce adsorbates that possess low vapor pressures.

1.6 Non-electrochemical characterization methods of self-assembled monolayers

SAMs have been subjected to nearly every known surface analytical method. Among the more frequently applied tools are contact angle, ellipsometry, surface IR (infrared) spectroscopy, surface enhanced Raman spectroscopy (SERS), X-ray photoelectron spectroscopy (XPS), Auger electron spectroscopy (AES), scanning electron microscopy (SEM), scanning tunneling (STM) and atomic force (AFM) microscopy.

Out of several methods mentioned above, surface enhanced Raman spectroscopy (SERS) is used in this work and it will be discussed in more detail later on.

1.7   Electrochemical characterization of self-assembled monolayers

Double-layer structure and capacitance

Electrode/electrolyte interfaces demonstrate a capacitance whose magnitude reflects the distribution of ions on the solution side of the interface. The electrolyte double layer is composed of the Helmholtz layer consisting of ions and solvent in physical contact with the electrode and the diffuse layer, which contains ions near the electrode whose concentrations deviate from bulk concentrations.

Interfacial capacitances are often measured via the charging current in a cyclic voltammogram. More comprehensive studies of capacitance behaviour are obtained by alternating current (*ac*) impedance measurements or *ac* voltammetry. A simple parallel-plate capacitor model shows that the reciprocal capacitance increases linearly with the thickness of the dielectric layer [78].

Electrochemical stripping and deposition of self-assembled monolayers

SAMs from thiols, disulfides and sulfides oppose desorption over a wide potential range, but at very negative/positive potentials and in strongly alkaline electrolytes they are desorbed quantitatively.

The potentials of the cathodic stripping peaks provide information about the strength of the metal-sulfur bond and the presence of any intermediate or weakly adsorbed states [80]. The desorbed thiols tend to remain near the electrode and are readily readsorbed when the electrode potential is shifted to a more positive value [78].

Blocking behaviour

Alkanethiol SAMs restrain faradaic processes such as electrode oxidation and the exchange of electrons between the electrode and solution redox couples. The property of this blocking is attributed to the compactly packed structure of the monolayer, which obstructs the approach of solution ions and molecules to the electrode surface. Electrostatic attraction or repulsion between surface moieties on the SAM and solution redox couples has a powerful effect on the blocking behaviour of

SAMs. Promising applications of blocking SAMs can be found in the areas of corrosion inhibition, nanoscale lithography and ion selective electrodes. However, closer examination of SAM-coated electrodes reveals the presence of pinholes (bare metal sites) and other defects, which allow a close approach of solution species [78].

Unfortunately, no procedure has been urbanized which consistently yields pinhole-free SAMs. For bulk solid metal electrodes, surfaces should be annealed, cleaned from organic contaminants and etched to expose fresh metal and to remove inorganic oxides, a potential source of pinholes.

1.8   Applications of self-assembled monolayers

SAMs offer an exceptional combination of physical properties that allow fundamental studies of interfacial chemistry, solvent-molecule interactions and self-organization. Their well-ordered arrays and ease of functionalization make them ideal model systems in many fields [30,81,82]. Understanding the process of self-assembly is beneficial for manipulating the physicochemical properties of interfaces (e.g. wetting, frictional or adhesive properties of the surface layer) for a variety of heterogeneous phenomena such as catalysis, corrosion inhibition and lubrication [83-86]. The flexible self-assembly technique has a number of applications such as chemical and biological sensors [87], efficient electronic and optical devices [88,89], nonlinear optical materials, artificial membrane [90], electron-transfer barriers [91], high-density memory devices and photopatterning methodology [92-97].

Also SAMs can be used either to provide model systems of organized functional molecules for studying the interfacial phenomena, such as electron transfer or redox behaviour [98], or to create models for studying the interfacial interactions, such as adhesion or molecular recognition [82].

1.9   Self-assembled monolayers of thiols and electrochemistry

In electrochemistry, the convenience of thiol-based SAMs arises from their ability to endure the electrochemical experiment. SAMs on electrodes are stable over a wide range of potentials and electrolyte compositions (especially aqueous electro-

lytes). They afford means of controlling the electrode/electrolyte interfacial properties and the accessibility of the electrode surface to solution molecules. SAMs also provide a means of attaching a diverse set of structures, ranging from modified monolayers to multilayers, to the electrode. There are some specific applications including the development of more selective and sensitive electrochemical sensors (especially biosensors), controlling of faradaic reaction mechanism and a better understanding of factors controlling electron transfer over long distances and under large driving forces.

In electrochemical applications, surface modification by SAMs is widely used. Since the electrochemical properties of the end group (and the backbone) can be varied relatively easy, the use of SAMs in electrochemistry continues to be admired. Generally, the electrochemical potential offers a broad range of possibilities not only from a chemical, but also from a more physical perspective [99].

Preparation of metal electrodes coated with monolayers of thiolates having electrochemically active groups has attracted interest as a method to attach special functions to the electrodes [100-104]. These uses are based on the relatively high stability of the self-assembled monolayer against mechanical, thermal and chemical treatments. This fact means that self-assembly of thiols can be controlled by variation of the potential of the metallic supports and this can be used for many exciting applications such as electrical control of wetting [105], electrochemical patterning [106,107] and preparation of sensor arrays [108].

To understand the interaction between the modified surface and the species present in the phase in contact, one requires the knowledge, at a molecular level, of three fundamental aspects simultaneously: (1) the chemisorption process; (2) the geometrical configuration of the modifier molecules on the surface and (3) the dependence of the modifier molecules on the external applied potential.

1.10 Aim of the Work

The present work aims to form self-assembled monolayers of 2-mercaptopyridine and 4-mercaptopyridine on the surface of a polycrystalline gold electrode.

The effect of the electrode potential, the electrolyte solution and the solvent on the adsorption process will be investigated.

The mode of surface bonding of the two mercaptopyridines on the surface of the polycrystalline gold electrode will also be studied.

The influence of self-assembled monolayers of 2- and 4-mercaptopyridines on electrodeposited layer of copper on the surface of the gold electrode will be electrochemically studied. The stability of these monolayers on gold electrode will also be examined in the presence of copper ions in the solution.

The mechanism of electron transfer reaction through the mercaptopyridine monolayers will be investigated. The effect of the conducting/insulator behaviour of these monolayers on the gold electrode will also be carried out which could behave as microarray electrode.

Finally, the application of the formed monolayers of 2- and 4-mercaptopyridine will be tested as corrosion inhibitors for a steel electrode in sodium chloride solution.

-Experimental-

2   Experimental

2.1   Cyclic Voltammetry

Cyclic voltammograms (CVs) were recorded with a polycrystalline gold disk (surface area is approximately 0.1 cm^2) embedded in epoxy as a working electrode in aqueous solutions of 0.5 **M** H_2SO_4, 0.1 **M** H_2SO_4 containing 1.0 **M** $CuSO_4$ and 1.0 **M** $HClO_4$ containing 10 **mM** $(NH_4)_2Fe(SO_4)_2 \cdot 6H_2O$ + 10 **mM** $(NH_4)Fe(SO_4)_2 \cdot 12H_2O$ as supporting electrolytes using a custom built potentiostat interfaced with a standard PC via an ADDA-converter card operating with custom-developed software. A gold sheet electrode is used as a counter electrode. Hg/Hg_2SO_4 in 0.1 **M** K_2SO_4 (MSE), its potential is 641 mV *vs* standard hydrogen electrode, and a reversible hydrogen electrode (RHE) in 1.0 **M** $HClO_4$ are used as reference electrodes. CVs were recorded in a H-cell separated by glass frits.

The working electrode is treated as follows: The Au electrode was polished with 0.3 µm α-Al_2O_3 then 0.05 µm α-Al_2O_3 then washed ultrasonically with water. Before chemical modification, the electrode was cleaned in 0.5 **M** H_2SO_4 by potential scanning between – 0.4 to 1.3 V *vs* MSE until a reproducible cyclic voltammogram was obtained. After cleaning, the electrode was rinsed with deionized water and immediately immersed into the solution of the mercaptopyridine for 3 minutes and then rinsed carefully with water to remove the non-chemisorbed species, if any.

2.2   Electrochemical Impedance Measurement (EIM)

Electrochemical impedance measurements were carried out by using a gold sphere electrode with a surface area of 0.13 cm^2 in aqueous solution of 1.0 **M** $HClO_4$ as a supporting electrolyte containing 10 **mM** $(NH_4)_2Fe(SO_4)_2 \cdot 6H_2O$ + 10 **mM** $(NH_4)Fe(SO_4)_2 \cdot 12H_2O$. A potentiostat solartron SI 1287 connected to frequency response analyzer SI 1255 interfaced to a PC with EIM software was used in the measurements.

The measurements were carried out at 0.7 V *vs* RHE in 1.0 **M** $HClO_4$ with potential amplitude 5 mV and a wide frequency range from 0.1 Hz to 100 KHz was used. Evaluation of the impedance data was performed assuming equivalent circuit with Boukamp software.

2.3   Surface Enhanced Raman Spectroscopy (SERS)

In situ surface enhanced Raman experiments were conducted in custom designed glass cells on a T64000 Raman spectrometer equipped with a 2D CCD camera cooled with liquid nitrogen. A COHERENT INNOVA 70 Kr^+ gas ion laser provided laser illumination. SER spectra were recorded using 647.1 nm exciting laser light. The laser power was always maintained at 50 mW at the surface of the electrode to avoid destruction of the monolayer. 0.5 **M** aqueous H_2SO_4 was used as an electrolyte solution and MSE and gold sheet electrode were used as reference and counter electrodes respectively.

Electrochemical roughening necessary to confer surface enhancement activity was performed. Roughening of the gold electrode (polycrystalline 99.99 %, polished down to 0.3 μm Al_2O_3) was performed in a separate cell with an aqueous solution of 0.1 **M** KCl by cycling the electrode potential between E_{SCE} = - 800 mV and E_{SCE} = 1650 mV for approximately 10 minutes [109]. A gold sheet and a saturated calomel electrode (SCE) were used as counter and reference electrodes respectively.

2.4   Corrosion Studies

A C60-steel disk electrode (0.61% C, max. 0.40% Si, 0.75% Mn, max. 0.40% Cr, max. 0.10% Mo, max. 0.40% Ni and max. 0.63% others) was used as a working electrode. It was manufactured as a cylindrical shape of 10 mm height. The electrode is surrounded with Teflon in a way to function as a disk electrode with 1.13 cm^2 exposed surface area. It was polished on a sand paper 1000 grade and then on a 13 μm α-Al_2O_3. A gold sheet electrode and a saturated calomel electrode were used as counter and reference electrodes respectively. 3.5% NaCl was used as a supporting electrolyte. The corrosion of the steel and the effect of the SAMs of the mercaptopyridines were studied by electrochemical impedance measurements.

2.5   Materials

Electrolyte solutions were prepared from 18 MΩ water (Seralpur Pro 90 c), 2-mercaptopyridine (Aldrich), 4-mercaptopyridine (Aldrich), sulphuric acid (Merck, G.R.), copper sulfate, perchloric acid (Acros, p.A.), potassium chloride (Merck, G.R.) ammonium iron (II) sulfate-6-hydrate (Riedel-de Haën AG), ammonium iron (III) sulfate-12-hydrate (Riedel-de Haën AG) and sodium chloride were used as received. 1 **mM** of 2- and 4-mercaptopyridine solutions were used in all electrochemical and SERS experiments.

All solutions were freshly prepared, purged with nitrogen (99.999%) except for corrosion studies. All measurements were performed at room temperature.

3 Results and discussion

3.1   Cyclic Voltammetry

The use of electrochemical techniques such as cyclic voltammetry provides a mean of investigating the energetics of the system and also for an indirect characterization of the processes taking place. The presence of co-adsorbed species would be anticipated to have a pronounced effect on the voltammetric features of the investigated system. Formation of organized molecular assemblies at electrode surfaces present an enormous scope to manipulate the interfacial architecture that holds the key to the proper understanding of several issues such as metal deposition, electron transfer, etc.

3.1.1   Electrochemical behaviour of a gold electrode in 0.5 M H_2SO_4

Fig. 4 shows the cyclic voltammogram (CV) of a bare polycrystalline gold electrode in 0.5 **M** H_2SO_4 in the potential range of 0.0 to + 1.3 V *vs* MSE at a scan rate of 100 mVs^{-1}.
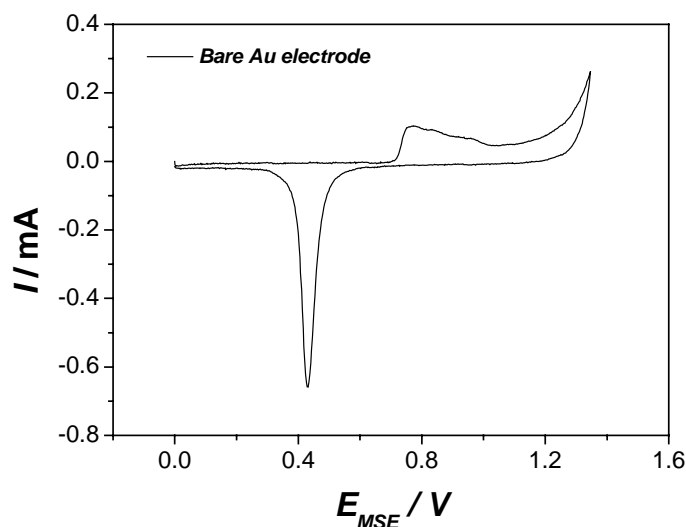

Fig. 4   CV of a bare polycrystalline Au electrode in 0.5 **M** H_2SO_4, dE/dt 100 mVs^{-1}.

It can be observed in the figure that during the anodic scan of the first cycle there is a peak at 0.76 V indicating gold oxide formation, which undergoes reduction at 0.43 V in the cathodic scan [110].

3.1.2 Electrochemical behaviour of 2-mercaptopyridine on gold electrode

Fig. 5 shows the CVs of a polycrystalline gold electrode pretreated with 1 **mM** solution of 2-mercaptopyridine (dissolved in water) in 0.5 **M** H_2SO_4. It is observed that during the anodic scan in the first cycle a broad peak at 1.16 V is formed. This rising current refers to two processes, which are the oxidation of the Au surface and the oxidation of 2MP. Again, during the cathodic scan of the first cycle, a Au oxide reduction peak occurs at 0.40 V whose peak height is considerably less than that resulting from a bare Au electrode under identical conditions. This suggests that the presence of adsorbed 2MP gives rise to a decrease of the gold oxide formation to a certain level and the main process that takes place might be the adsorbate oxidation [64,99,110].
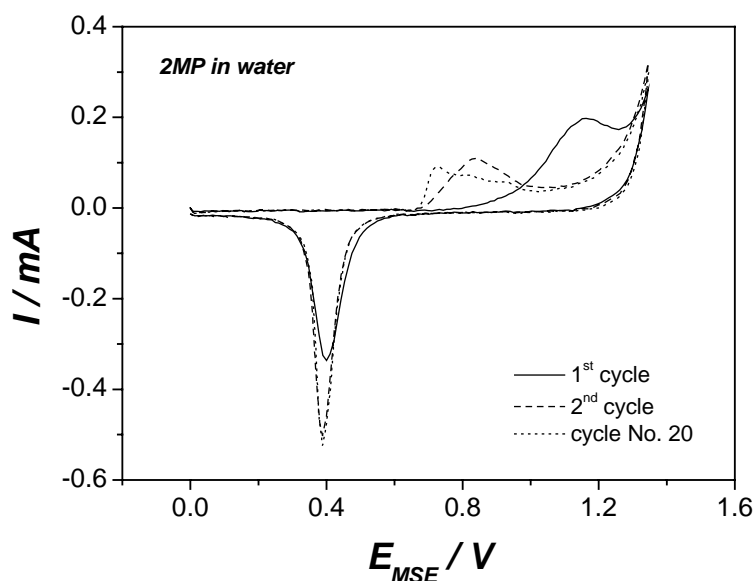

Fig. 5   CVs of a polycrystalline gold electrode pretreated with 2MP (dissolved in water) in 0.5 **M** H_2SO_4, dE /dt 100 mVs[-1].

During the second cycle, the current at 1.16 V decreases and a separate peak that resolves itself distinctly with increasing number of cycles, corresponding to Au oxida-

tion, could be noticed at around 0.84 V. This peak shifted to more negative potential with the subsequent cycling. In addition, with increasing number of cycles, the peak current due to the Au oxide reduction also increases. This suggests that during the first scan the oxidation of a Au surface is minimal owing to the presence of a 2MP layer. Subsequent cycles expose the Au surface, possibly due to the removal of the 2MP layer to the solution facilitating the formation of Au oxide and its reduction [110]. This tendency for Au oxide formation followed by its reduction increases gradually with increasing the number of cycles. This indicates that 2MP can be oxidized in an acidic medium on Au electrode [64].

The adsorption process for MPs suggests a net electron transfer from the sulfur atom to the metal as part of the monolayer formation process [111]. However, the sulfur atom behaves as an electron acceptor when it is bonded to gold [111] due to the large difference between the electronegativities of sulfur and gold [112]. The overall reaction is frequently expressed as eq. 1 [75,113-116].

$$Au + RSH = Au\text{-}SR + \tfrac{1}{2}\,H_2 \qquad \text{eq. 1}$$
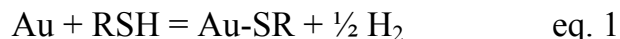
Although 2MP probably adsorbs primarily through the sulfur atom, the presence of the pyridine ring, with the nitrogen atom in the "ortho" position, could give rise to the formation of a chelate with the gold surface, thus giving rise to more strongly adsorbed layer [64-67]. The formed surface chelate of type S–Au–N is shown in (Fig. 6) [67].
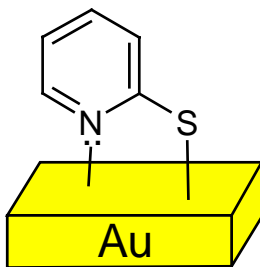
Fig. 6   The chelate structure of 2-mercaptopyridine with Au surface

It is also possible that 2MP can be dimerized through the S atom to form bis-(2-pyridyl)disulfide as shown in equation 2, but the formed chelate structure hinders the dimer formation [67].

eq. 2
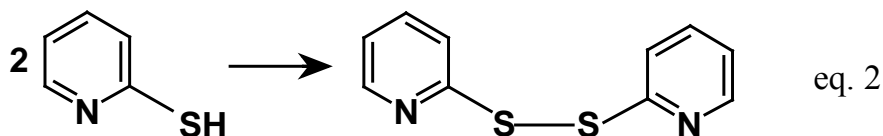
When the polycrystalline Au electrode is pretreated with 1 **mM** solution of 2MP (dissolved in 0.1 **M** H_2SO_4) the CVs in 0.5 **M** H_2SO_4 (Fig. 7) show the same interesting features still exist, but with a slightly negative shift in the oxidation peak as compared with 2MP in water. This behaviour might be due to weak bonded 2MP in 0.1 **M** H_2SO_4, since in this solution the nitrogen of the pyridine ring is protonated, as a result the strength of interaction is dominated by the sulfur atom [64,66].
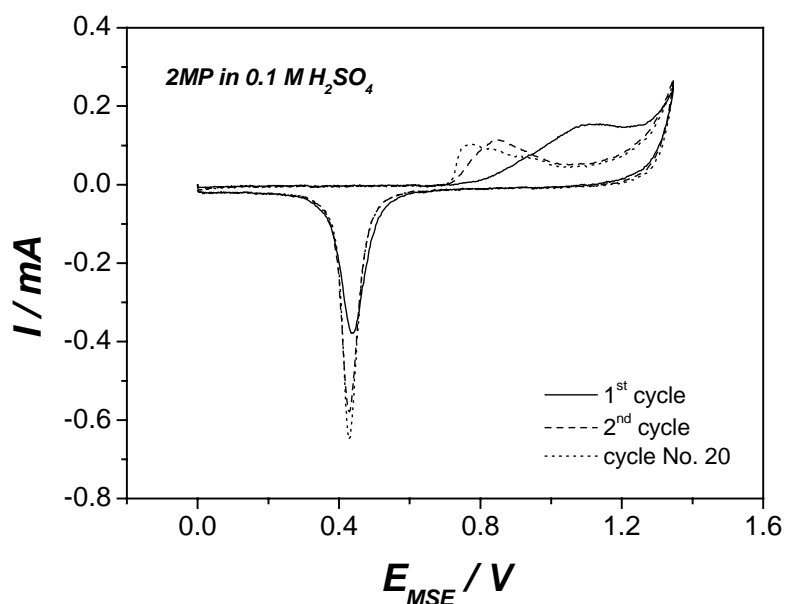
Fig. 7   CVs of a polycrystalline gold electrode pretreated with 2MP (dissolved in 0.1 **M** H_2SO_4) in 0.5 **M** H_2SO_4, dE/dt 100 mVs^{-1}.

3.1.3 Electrochemical behaviour of 4-mercaptopyridine on gold electrode

Fig. 8 shows CVs of a polycrystalline gold electrode pretreated with 1 **mM** solution of 4-mercaptopyridine (dissolved in water) in 0.5 **M** H_2SO_4.

It is observed during the anodic scan in the first cycle that a current plateau at 0.93 V is formed. The increasing current might be due to the oxidation of both 4MP monolayer and the Au surface [64,99]. This plateau is shifted to a more negative potential compared with the case of 2MP in water. It means less inhibition of Au oxide formation in case of 4MP [54,64].

As mentioned before for 2MP, during the cathodic scan of the first cycle, a gold oxide reduction peak occurs at 0.42 V whose peak height is considerably less than that resulting from a bare Au electrode under identical conditions suggesting that the 4MP monolayer decreases of gold oxide formation and that the main process that is the adsorbate oxidation [64,115].

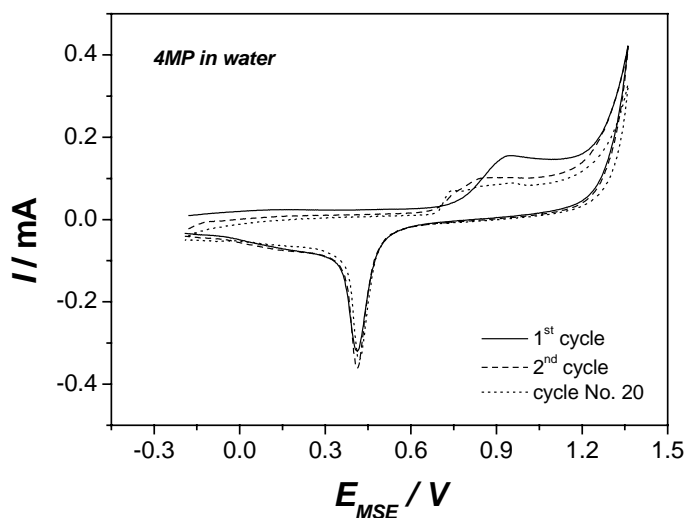**Fig. 8**   CVs of a polycrystalline gold electrode pretreated with 4MP (dissolved in water) in 0.5 **M** H_2SO_4, dE /dt 100 mVs^{-1}.

In the second cycle, the current at 0.93 V decreases and a broad peak appears at around 0.83V, which is shifted to more negative potential with increasing the numbers of the cycles. Additionally the peak height of the Au oxide reduction increases with

subsequent cycling. This suggests that when 4MP adsorbed on the Au electrode, the Au oxide formation is decreased. With subsequent cycles, due to the removal of the 4MP layer, the formation of Au oxide and its reduction is facilitated [110]. The tendency of Au oxide formation followed by its reduction increases with increasing the number of cycles. This indicates that also 4MP can be oxidized in an acidic medium on Au electrode [64].

In the case of 4MP, since the nitrogen atom is in the "para" position the chelate structure cannot form. Thus, the bonding to the surface is solely through the sulfur atom. This may result in a diminishing of the interaction of the adsorbed layer with the surface of the electrode [64,66,67]. The formation of the chelate (S-Au-N) in case of 2MP diminishes the negative charge on the S-atom. Therefore 2MP is adsorbed more strongly, due to the chelate formation, than 4MP. However, the S-metal bond is stronger in 4MP than in 2MP [67]. The formation of the S-Au bond proved by surface enhanced Raman spectroscopy will be intensively discussed in section 3.3.

It was also concluded that 4MP binds to the electrode surface through the sulfur atom (normal geometry) in almost vertical orientation as in Fig. 9 [61,64]. In this case the packing density is larger than that for 2MP. There is also a small probability that 4MP binds to the surface through a nitrogen atom (out of normal geometry) as shown in Fig. 9 [64,67].
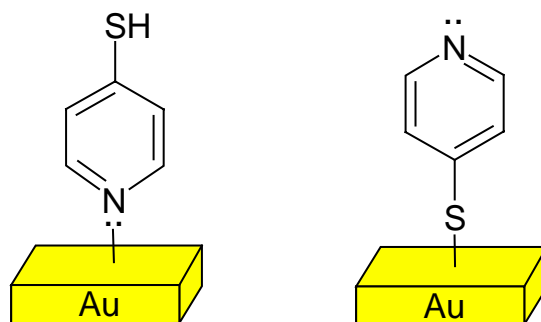
Fig. 9   The possibilities of 4-mercaptopyridine bonding with the Au surface.

On the other hand, 4MP dissolved in water can form bis-(4-pyridyl)disulfide as in equation 3, which can be reduced easily and completely back to 4MP [49,66,67,

117]. In addition, it has been proposed that it can undergo the coupling reaction depicted in equation 4 [49]. The formation of this last product would be favored in acid medium.

bis-(4-pyridyl)disulfide   eq. 3

eq. 4
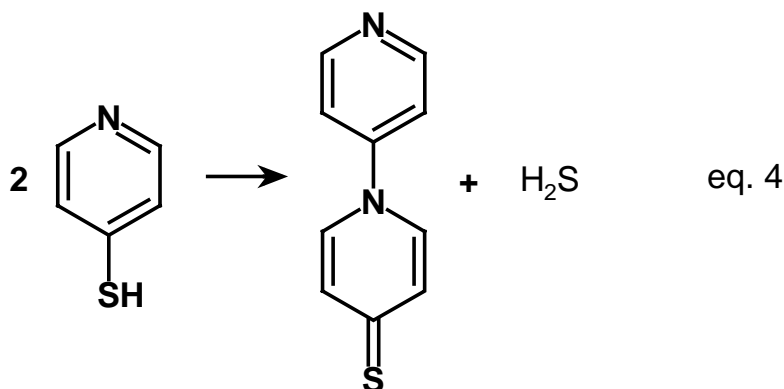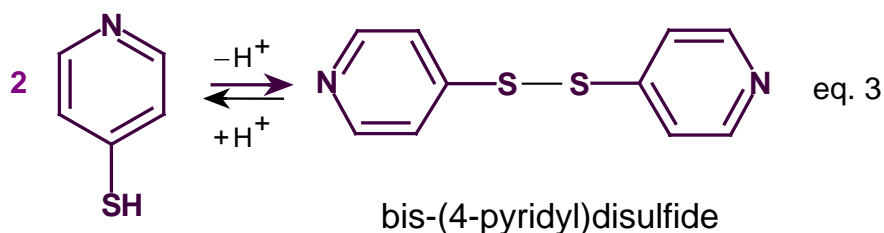
In fact both 2MP and 4MP are electrochemically active and can furthermore undergo side reactions.

When 4MP (in 0.1 **M** H_2SO_4) is adsorbed on Au electrode surface, the cyclic voltammograms (Fig. 10) show a similar behaviour to that described for 4MP adsorbed from water, with the exception that the oxidation peak is slightly shifted to the negative potential. In addition, the height of the reduction peak is slightly lower than obtained in the case of 4MP dissolved in water. It is also lower than that for 2MP either in water or in 0.1 **M** H_2SO_4. This behaviour might be due to weaker interaction between Au surface and the bonded 4MP dissolved in 0.1 **M** H_2SO_4 [64,66]. In 0.5 **M** H_2SO_4 the N-atom is protonated. Such protonation would cause (by inductive effects) a weakening of the sulfur-gold bond, besides diminishing the possibility of adsorption onto the electrode surface [64,66,67].
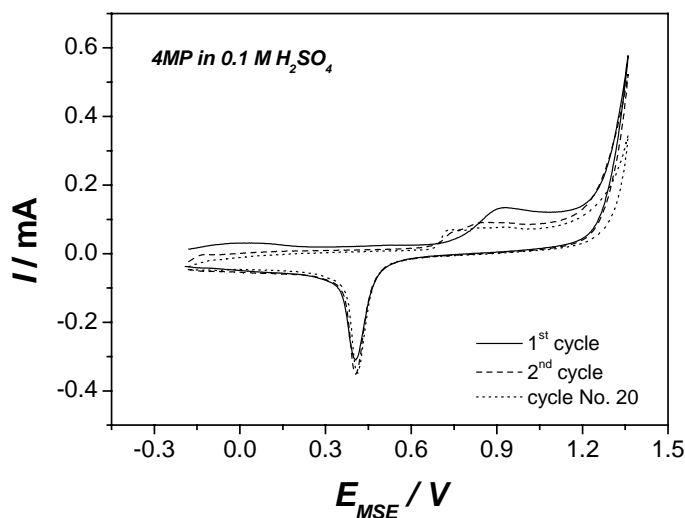
Fig. 10   CVs of a polycrystalline gold electrode pretreated with 4MP (dissolved in 0.1 **M** H_2SO_4) in 0.5 **M** H_2SO_4, dE /dt 100 mVs^{-1}.

In summary, when 2MP is deposited on the Au electrode surface from both media the formation of Au oxide is more inhibited than in the case of 4MP and the inhibition in the neutral is higher than in the acidic medium for both adsorbates. This behaviour is similar to that described by Alonso et al. [54] for polycrystalline platinum electrode.

3.1.4 Electrodeposition of copper on gold electrode

Electrochemical techniques such as cyclic voltammetry allows the characterization of processes taking place during the electrodeposition of metals in the presence and absence of coadsorbed species, reflecting the interaction existing between the coadsorbates, the electrode surface and the metal overlayer [118-124]. Under the assumption that two electrons are transferred per copper atom, Wieckowski and co-workers [121] conclude that nearly a closed-packed monolayer of copper is formed on the metal surface. The adsorption of numerous organic species on the electrode surface has been investigated, showing that they are able to hinder or even inhibit the electrodeposition of copper and silver onto metal substrates depending on the strength of adsorption [49,65,124]. Moreover, it has been established that the SAMs of mercaptopyridines are able to displace copper and silver monolayers [54,66,67] deposited on gold [65] and platinum [64] electrodes.

The copper deposition on a polycrystalline gold electrode from 1 **mM** $CuSO_4$ solution in the absence of the monolayer is displayed in Fig. 11.
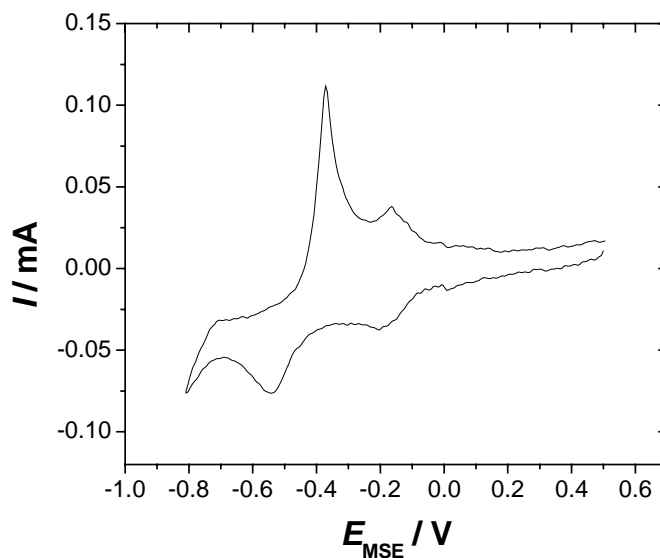
Fig. 11 Underpotential and overpotential deposition of copper from 1 **mM** $CuSO_4$ solution in 0.1 **M** aqueous H_2SO_4 on a polycrystalline gold electrode, dE/dt 50 mVs^{-1}.

The potential was scanned in the negative direction at 50 mVs^{-1} from a starting point of + 0.5 V *vs* MSE. The CV illustrates both underpotential deposition (UPD) and overpotential deposition (OPD) regions.

On the initial cathodic scan, two peaks at – 0.20 corresponding to copper UPD and at – 0.54 V corresponding to copper OPD are observed. In the subsequent positive scan, two features are observed for the stripping of the electrodeposited copper: a sharp peak at a potential of – 0.37 V corresponding to the removal of bulk copper (OPD) and a peak at – 0.17 V corresponding to the stripping of copper UPD [66].

The influence of 2MP and 4MP monolayers on electrodeposition of copper on a polycrystalline gold electrode has been also studied. Additionally the interaction of these adsorbates with the gold electrode covered with an initially deposited copper ad-layer is also investigated.

3.1.5   Copper deposition on gold electrode pretreated with 2-mercaptopyridine

Fig. 12 shows the CVs for copper deposition on a gold electrode and on the gold electrode pretreated with 1 **mM** solution of 2MP in water. It can be observed from the figure that the copper deposition is inhibited on the Au surface. It can be also noticed that the peak potentials for UPD and OPD are the same as that for the copper deposition onto a bare gold electrode, with a decrease of the peak current, while both peaks for OPD and UPD stripping are shifted in the positive direction reflecting the presence of the 2MP on the surface. This suggested that the strength of interaction between the sulfur atom and the Au surface is greater than that between the deposited copper and the surface. The presence of very weak peaks that indicated the presence of copper might be attributed to the free sites (defects) of the 2MP monolayer, which allow copper adatoms to be deposited on the surface [64,66].

Fig. 12   Deposition of copper from 1 **mM** copper solution in 0.1 **M** aqueous H_2SO_4
solution onto a polycrystalline Au electrode (solid line) and onto a Au elec-
trode pretreated with a 1 **mM** solution of 2MP in water (dashed line), d*E*/d*t*
50 mVs^{-1}.

Table 1 (see page 43) summarizes the peak potentials associated with copper
deposition and stripping on a bare gold electrode and on gold electrode pretreated
with 2MP and 4MP dissolved in either water or in 0.1 **M** H_2SO_4.

When an electrode is pretreated with a 1 **mM** solution of 2MP in 0.1 **M** aque-
ous H_2SO_4, the CV (Fig. 13) shows a slightly greater copper deposition more than in
the case of 2MP dissolved in water. In the cathodic scan the peak potential of the UPD
is the same as in the case of the bare electrode and gold electrode pretreated with 2MP
in water while the OPD is shifted in the negative direction. In addition, the stripping
of both OPD and UPD is shifted in the positive direction (see Table 1 page 43). This
can be explained by the chelate formation in case of 2MP in water, which gives rise to
stronger adsorption of the 2MP monolayer thus preventing more copper to be depos-
ited on the Au surface [64-67].

40

Fig. 13   Deposition of copper from 1 **mM** copper solution in 0.1 **M** aqueous H_2SO_4 solution onto a polycrystalline Au electrode (solid line) and onto a Au electrode pretreated with a 1 **mM** solution of 2MP in 0.1 **M** aqueous H_2SO_4 (dashed line), dE/dt 50 mVs^{-1}.

3.1.6   Copper deposition on gold electrode pretreated with 4-mercaptopyridine

If a gold electrode is pretreated with 4MP in water the electrodeposition of Cu is diminished as shown in (Fig. 14). In the cathodic scan the copper UPD is shown to appear at – 0.21 V and the copper OPD at – 0.66 V. In the subsequent anodic scan two peaks at – 0.33 and at – 0.10 V indicating the OPD and UPD stripping of copper are observed respectively.

In comparison with 2MP, the presence of 4MP monolayer allows more Cu adatoms to approach the Au surface (see Table 1 page 43), which might be indicated from the height of the stripping peaks in both cases and the shift of the copper OPD peak to a more negative value. This may be attributed to the possibility of the 4MP molecules to bind to the Au surface only through the S-atom since the presence of the N-atom in the para position precludes the chelate formation as in the case of 2MP.
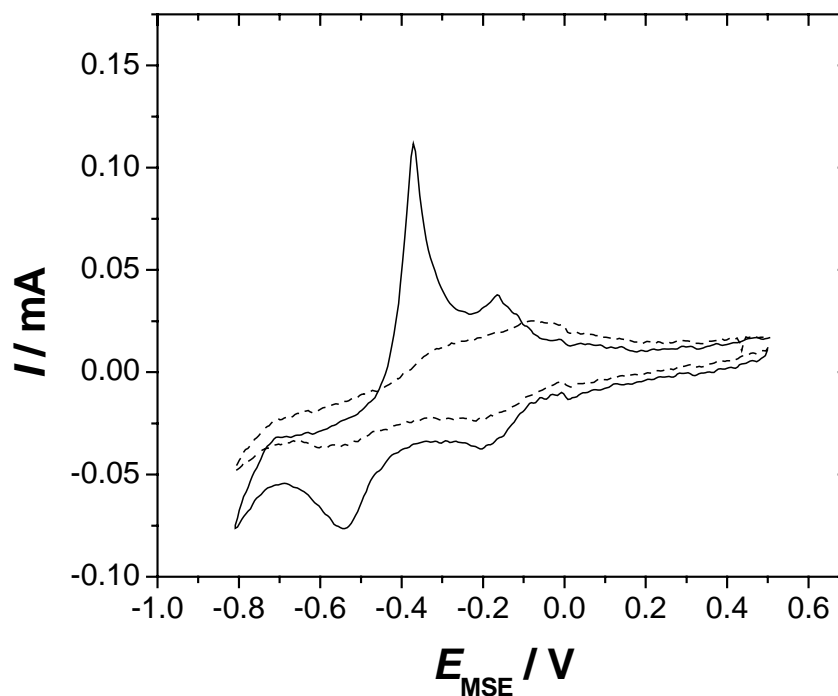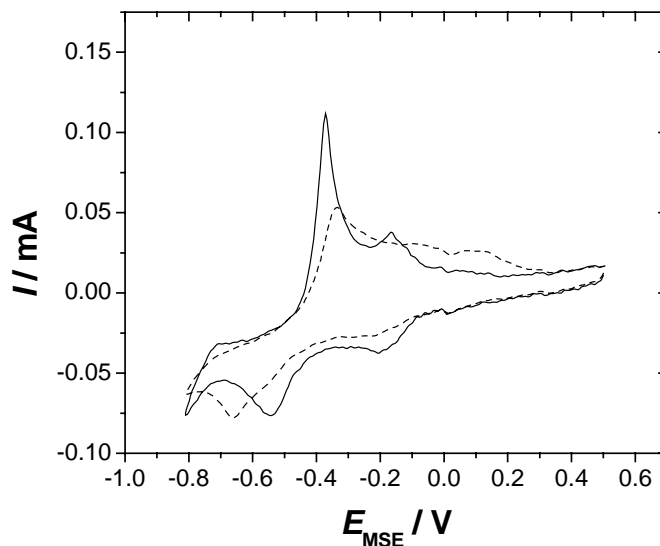
Fig. 14 Deposition of copper from 1 **mM** copper solution in 0.1 **M** aqueous H_2SO_4 solution onto a polycrystalline Au electrode (solid line) and onto a Au electrode pretreated with a 1 **mM** solution of 4MP in water (dashed line), dE/dt 50 mVs^{-1}.

The cyclic voltammogram of the Au electrode pretreated with 4MP dissolved in 0.1 **M** aqueous H_2SO_4 is shown in Fig. 15. Under these conditions, a peak at –0.20 V is obtained in the UPD region corresponding to copper deposition on sites free of 4MP. The OPD of copper takes place at a potential of – 0.69 V which is more negative than in the case of the absence of 4MP monolayer (see Table 1 page 43), implying that the process is less favored. In the anodic scan, peaks at – 0.33 and – 0.08 V corresponding to OPD and UPD stripping respectively are observed. The presence of 4MP (deposited from H_2SO_4) inhibits the UPD stripping, delaying it 90 mV to a more positive potential.

In comparison with 4MP dissolved in water (see Table 1 page 43), the OPD is shifted to a more negative potential in the case of 4MP deposited from H_2SO_4. This behaviour may be attributed to the protonation of the N-atom of 4MP in the acidic solvent, which is located para to the S-atom, such protonation would (by inductive effect) cause a weakening of the S-Au bond [64,66].
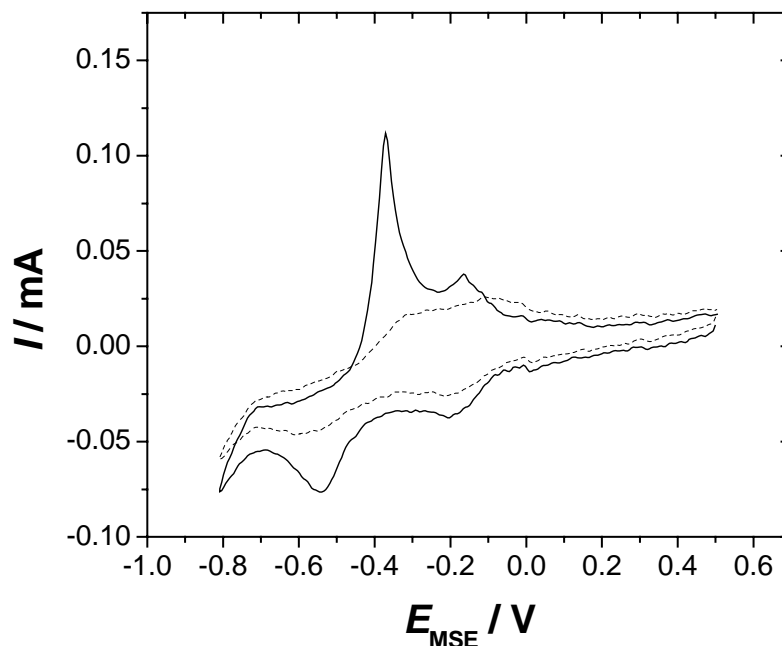
42
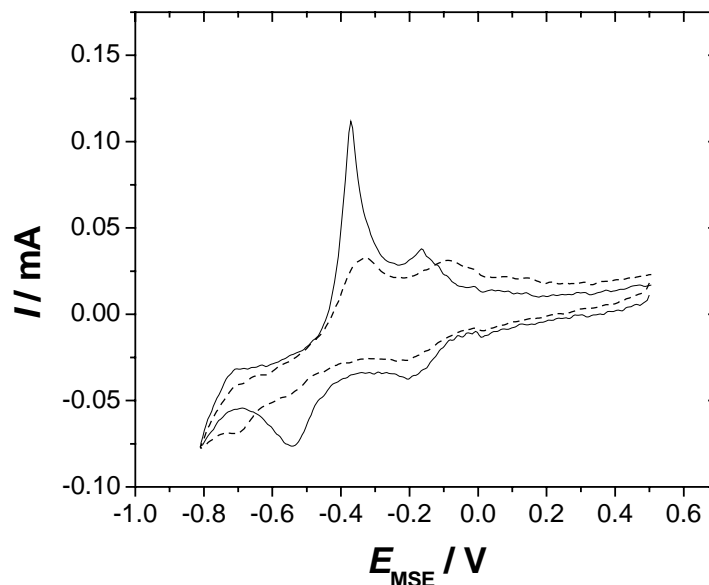
Fig. 15 Deposition of copper from 1 **mM** copper solution in 0.1 **M** aqueous H_2SO_4 solution onto a polycrystalline Au electrode (solid line) and onto a Au electrode pretreated with a 1 **mM** 4MP solution in 0.1 **M** aqueous H_2SO_4 (dashed line), dE/dt 50 mVs^{-1}.

Table 1: Deposition and stripping potentials (*vs* MSE) for copper deposition on gold in the absence and presence of SAMs.

SAMs	UPD$_{dep.}$	OPD$_{dep.}$	OPD$_{str.}$	UPD$_{str.}$
Bare Au	-0.20	-0.54	-0.37	-0.17
2MP (water)	-0.20	-0.54	-0.25	-0.06
2MP (acid)	-0.20	-0.59	-0.29	-0.09
4MP (water)	-0.20	-0.66	-0.33	-0.10
4MP (acid)	-0.20	-0.69	-0.33	-0.08

3.1.7 **Displacement of electrodeposited copper on gold by 2-mercaptopyridine**

When a copper monolayer is electrodeposited on a polycrystalline gold electrode and subsequently exposed to a solution of 2MP in H_2SO_4 (dashed line in Fig. 16), the copper monolayer is partially stripped as can be observed in the anodic scan.

This suggests that the strength of interaction between the S-atom and the gold surface is greater than that between the deposited copper and the surface.
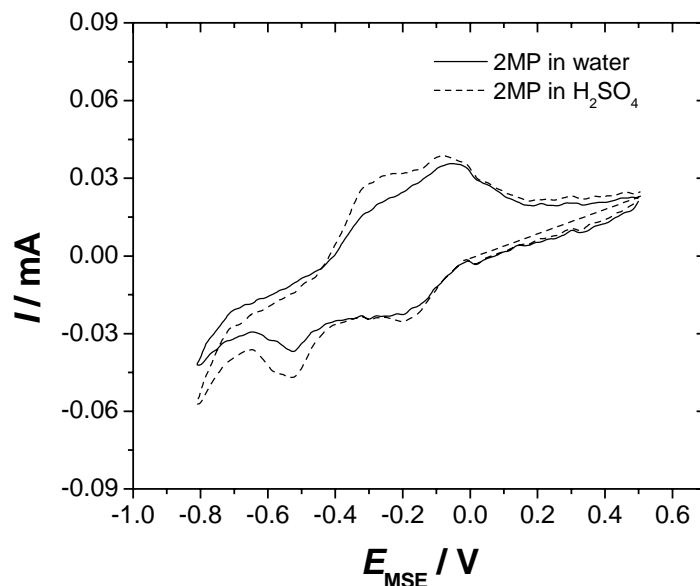
Fig. 16 CVs of a polycrystalline gold electrode with an initially deposited Cu ad-
layer in 0.1 **M** aqueous H_2SO_4 after immersion in 2MP solutions, dE/dt 50
mVs^{-1}.

If the gold electrode with an initially deposited copper is immersed in 2MP so-
lution in water, the displacement of copper is more than in case of 2MP dissolved in
H_2SO_4. In this case the N-atom of the pyridine ring is not protonated, resulting in an
increase in the strength of interaction between the adsorbed 2MP monolayer and the
electrode so that 2MP became able to displace more electrodeposited copper.

3.1.8 Displacement of electrodeposited copper on gold by 4-mercaptopyridine

When a gold electrode with an electrodeposited Cu adlayer is immersed in 4MP
solution in water or H_2SO_4 (Fig. 17), the anodic scan shows the stripping of the Cu
adlayer.
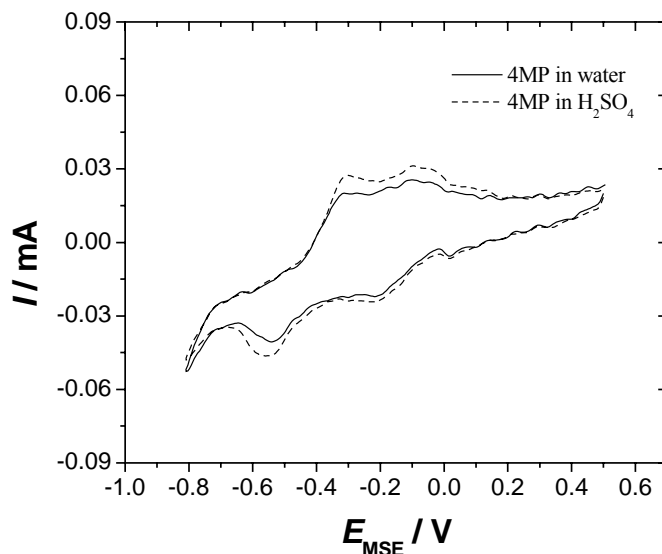
Fig. 17 CVs of a polycrystalline gold electrode with an initially deposited Cu ad-
layer in 0.1 **M** aqueous H_2SO_4 solution after immersion in 2MP solutions,
dE/dt 50 mVs^{-1}.

The structure of 4MP precludes the formation of a chelate with the Au surface,
as in the case of 2MP. Thus, bonding to the surface is solely through the sulfur atom.
This may result in a diminution of the interaction of the adsorbed layer with the elec-
trode so that 4MP displaces less copper. Besides, more copper is displaced by 4MP in
water than by 4MP in 0.1 **M** aqueous H_2SO_4 solution because in the acidic solvent the
N-atom is protonated. Since the N-atom is located para to the S-atom such protonation
would (by inductive effect) cause a weakening of the S-Au bond, diminishing the
amount of displaced copper.

3.1.9   Electron transfer kinetics of the redox reaction

Electrochemical techniques such as cyclic voltammetry and electrochemical impedance measurements, which will be discussed in more details in the next sections, are suitable techniques for the investigation of the structure and the electrochemical properties of the SAMs and for studying the fast interfacial processes. These techniques give useful information on the distribution of defects in the formed monolayers, the properties of the coupled redox probes, the kinetics and mechanism of the monolayer formation process, and the surface coverage, etc. [31,69,125-129]. The methodologies used with these techniques are always based on the comparison of the results obtained with the unmodified and SAM-modified electrode substrate.

3.1.10   Influence of 2-mercaptopyridine on electron transfer process

Fig. 18 shows the CVs of a gold electrode in 1.0 **M** aqueous $HClO_4$ solution containing $Fe^{3+/2+}$ redox couple in absence and presence of 2MP monolayer deposited from water in the potential range of 0.0 to + 1.5 V *vs* RHE at dE/dt of 100 mV s^{-1}.

It can be observed from the figure that a well-defined CV characteristic of a diffusion-limited redox process is obtained for the bare gold electrode showing a quasi-reversible behaviour with peak-to-peak separation (ΔE_p) of 120 mV [130]. For the electrochemically reversible process the equilibrium is maintained throughout the potential scan (equilibrium requires that the surface concentrations of O and R, where O and R are the oxidants and the reductants respectively, are maintained at the values required by the Nernst equation).

The reversible process is characterized by the following parameters:

1.   The peak potential separation $\Delta E_p = E_{pc} - E_{pa} = 58/n$ mV at all scan rates at 25°C (where E_{pc} and E_{pa} are the cathodic and the anodic peak potentials respectively and n is the number of electrons transferred/molecule).

2.   The current ratio $I_{pa} / I_{pc} = 1$ at all scan rates (where I_{pa} and I_{pc} are the anodic and the cathodic peak currents respectively).

3. The peak current function $I_p / v^{1/2}$ is independent of v (where v is the scan rate)

4. The peak current is given by the Randles-Sevcik relationship:

$$I_p = 2.69 \times 10^5 \, n^{3/2} \, A \, c \, D^{1/2} \, v^{1/2} \qquad \text{eq. 5}$$

where A is electrode surface area (0.13 cm^2), c is the concentration (mol L^{-1}) and D is the diffusion coefficient for the redox probe (cm^2 s^{-1}). The value of D calculated for Fe$^{3+/2+}$ redox couple using equation 5 is 3.45×10^{-7} cm^2 s^{-1}.
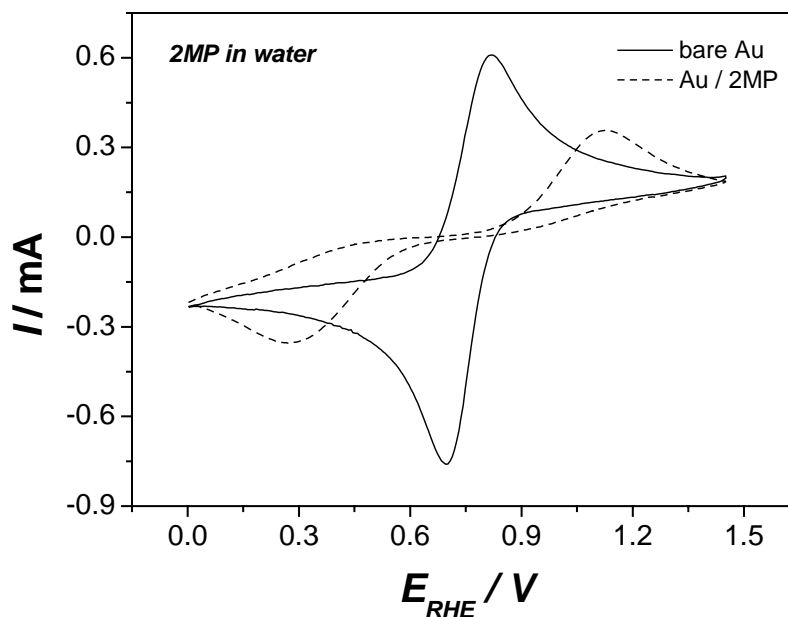
Fig. 18 CVs of a gold electrode in 1.0 **M** aqueous HClO$_4$ solution containing Fe$^{3+/2+}$ redox couple before and after immersion in 2MP solution in water, dE/dt 100 mV s^{-1}.

The midpoint potential (E_m) or the formal potential (E_f) can also be calculated as $E_m = (E_{pa} + E_{pc}) / 2$ [131]. The calculated E_m was found to be 760 mV vs RHE. The current ratio is unity within experimental error. All the above parameters are calculated and listed in Table 2 (see page 53).

The efficiency of the monolayer in blocking the heterogeneous electron transfer (ET) reaction can be estimated by the kinetics of the redox probes, as expressed by the

peak-to-peak separation (ΔE_p) [69]. When the 2MP layer, which has pinholes that allow the electron transfer through the monolayer, is adsorbed on the surface of the electrode, one can notice an obvious decrease in the cathodic and the anodic peak currents and an increase of the ΔE_p to a value of 847 mV. A significant positive potential shift for the anodic current peak and a negative potential shift for the cathodic current peak can be observed. The current ratio is close to unity. The value of E_m is 703 mV, which is less positive than the value of 760 mV (*vs* RHE) observed for the bare Au electrode. Assuming that the Randles-Sevcik relationship (eq.5) is applicable, it can give a value for the effective diffusion coefficient ($D_{eff.}$) of 1.06×10^{-7} cm^2 s^{-1}. This clearly indicates that the electrode surface was covered with a compact monolayer of 2MP, which creates a barrier decreasing the electron transfer process.

Pinholes are a kind of defect in thiol monolayers, which are the result of imperfect adsorption of the thiol molecule to the Au surface during the self-assembling step and/or subsequent loss of the formed monolayer during rinsing, storage or use. However, these pinholes are active sites in the formed monolayer. Concequently, the gold electrode modified with MPs behaves as a microarray electrode allowing molecules and ions from the electrolyte to reach the electrode surface [130,132-137]. Moreover, the π-electrons present in the molecules can further help the ET across the monolayers [138]. In fact, it has been generally observed that the organothiol SAM may or may not present some defects or pinholes on the surface, depending on the interaction between the adjacent molecules [134]. All the obtained values for Au electrode modified with 2MP deposited from water are listed in Table 2 (see page 53).

Porter et al. [31] have suggested that ET of electroactive species at the SAMs covered electrodes could occur in three ways: (1) the electron could transfer through the film via a tunneling process, (2) the electroactive species could permeate through the monolayer and react at the electrode surface and (3) the electroactive species could diffuse to a bare spot, a pinhole, on the electrode. Sur et al. [139] suggested that the redox reactions could take place through either or both of the following processes occurring in parallel:

1. Diffusion of the redox species through the pinholes and access to the electrode surface followed by electron transfer reaction.

2. Permeation of the redox molecule through the assembly and access to a region close to the electrode surface. This is followed by ET through tunneling process.

If 2MP is deposited from 0.1 **M** aqueous H_2SO_4 on Au surface (Fig. 19) there is a decrease in the cathodic and the anodic peak currents and an increase of the ΔE_p (731 V *vs* RHE) compared with the bare Au electrode. A significant positive potential shift for the anodic peak and a negative potential shift for the cathodic peak can be observed. The current ratio is close to unity. Assuming that the Randles-Sevcik relationship is applicable, it can give a value for $D_{eff.}$ of 1.58×10^{-7} $cm^2 s^{-1}$. All the obtained values for the Au electrode modified with 2MP deposited from 0.1 **M** H_2SO_4 are listed in Table 2 (see page 53).

Fig. 19 CVs of a polycrystalline gold electrode in 1.0 **M** aqueous $HClO_4$ containing the redox couple in the presence and absence of 2MP monolayer deposited from 0.1 **M** aqueous H_2SO_4, dE/dt 100 mV s^{-1}.

On comparison with 2MP dissolved in water (Table 2 page 53), the value of ΔE_p is lower and the value of E_m is higher in the case of 2MP dissolved in acid. Also the peak current is higher in the latter case. Additionally the anodic peak is shifted to

more negative potential. This indicates that the ET reaction is less hindert in the case of 2MP dissolved in acidic solution [130-133].

In acidic solvent the N-atom of the 2MP is protonated. It is proposed that two effects, which exist at the same time, are considered to be responsible for the charge transfer process. First, there will be a repulsive interaction between the positively charged monolayer and the positively charged redox probes. Second, there is a repulsion among the positively charged monolayer molecules that results in a less compact monolayer. The latter interaction leads to the formation of open channels in the monolayer, which makes it easier for the redox probe to penetrate the monolayer. The latter effect is dominating in charge transfer (CT) process, although the electrostatic repulsion still exists between $Fe^{3+/2+}$ and the positively charged 2MP monolayer, which explains the increase of the peak currents of 2MP dissolved in acidic solution compared with that of 2MP dissolved in water [140].

Berchmans et al. [141] rationalized the charge transfer response yielded by Au/SAM towards the positively charged $Fe^{3+/2+}$ redox system on the basis of the inner sphere electron-transfer character. Thus the thin, compact and impervious monolayers were visualized to effectively prevent the direct access of the redox couple $Fe^{3+/2+}$ to Au electrode surface, which was an essential prerequisite in inner sphere ET reactions. Further study by Zhou et al. [132] showed that the heterogeneous ET of the positively charged redox probe is very difficult in acidic medium

3.1.11 Influence of 4-mercaptopyridine on the electron transfer process

Fig. 20 shows the CVs of a polycrystalline gold electrode in 1.0 **M** aqueous $HClO_4$ containing $Fe^{3+/2+}$ in the absence and in presence of 4MP monolayer deposited from water in the potential range from 0.0 to + 1.5 V *vs* RHE.

It is observed that when 4MP is deposited from water on the Au electrode surface there is a decrease in both cathodic and anodic peak currents. A significant positive potential shift for the anodic current peak can be observed, whereas a negative potential shift occurred for the cathodic current peak. A value of 947 mV is calculated for ΔE_p. A value of 810 mV *vs* RHE, which is higher than the value of 760 mV for the bare

Au electrode, is obtained for E_m. Assuming that the Randles-Sevcik relationship is applicable, it can give a value for $D_{eff.}$ of 1.00×10^{-7} cm^{2}s^{-1}. All the obtained values for Au electrode modified with 4MP deposited from water are listed in Table 2 (see page 53).
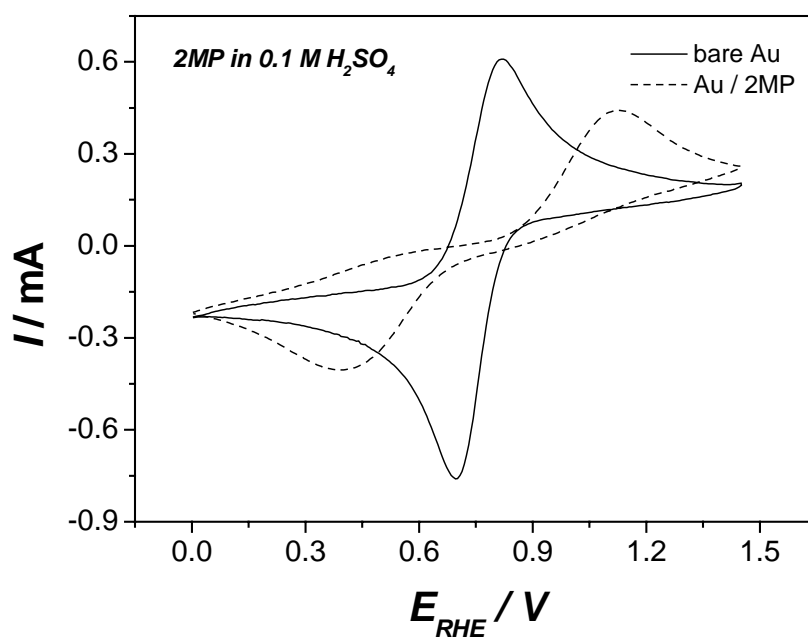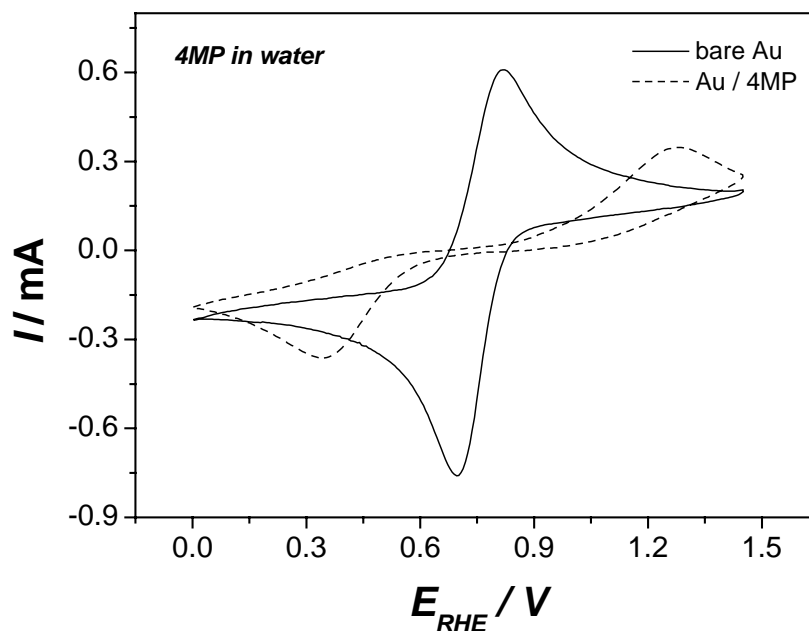

Fig. 20 CVs of a gold electrode in 1.0 **M** aqueous HClO$_4$ containing Fe$^{3+/2+}$ before and after immersion in 4MP solution in water, dE /dt 100 mV s^{-1}.

These differences between the bare Au electrode and the modified electrode with 4MP are due to the fact that in HClO$_4$ (electrolyte) solution the N-atom of 4MP is protonated, which leads to repulsive interaction between the positively charged monolayer molecules and the positively charged redox probe and repulsion among the positively charged monolayer molecules. This leads to the formation of open channels in the monolayer that allows the redox probe to penetrate the monolayer [141].

Compared with 2MP (Fig. 18), it was found that 4MP hinder the heterogeneous ET reaction stronger than 2MP. Since the packing density for 4MP is suggested [64,67] to be higher than that for 2MP, the number of pinholes might be lower in 4MP, which means less active sites are available for the ET reaction.

As shown in <u>Fig. 21</u>, when 4MP is deposited from 0.1 **M** aqueous H_2SO_4 on the Au electrode surface there is a decrease in the cathodic and anodic peak currents. A significant positive potential shift for the anodic current peak and a negative potential shift for the cathodic current peak can be observed. The current ratio is close to unity. For more details see Table 2 (see page 53).
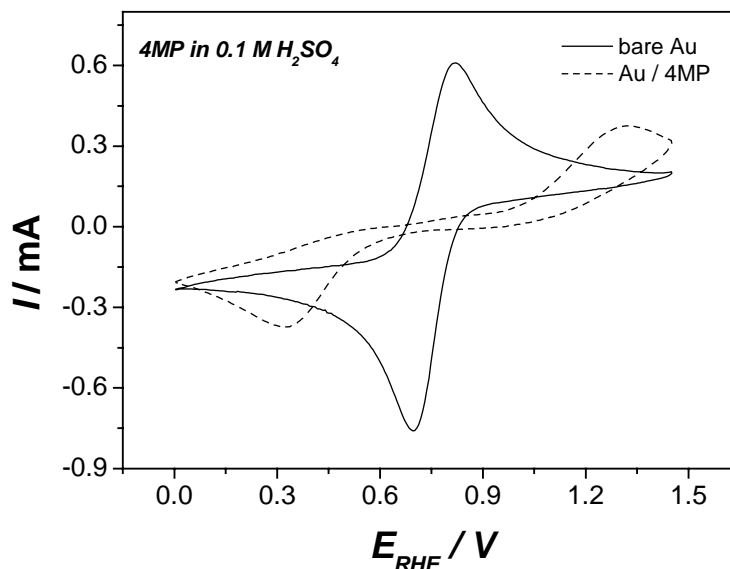
Fig. 21 CVs of a polycrystalline gold electrode before and after immersion in 4MP solution in 0.1 **M** aqeous H_2SO_4. Same conditions as in <u>Fig.20</u>.

In comparison with the case of 4MP dissolved in water (Table 2 page 53), it can be noticed that the ET reaction is more retarded in the case of 4MP dissolved in acidic solution depending on the values of the ΔE_p and the I_{pc} [130-133]. This can be explained as when 4MP is deposited from 0.1 **M** aqueous H_2SO_4 all the N-atoms will be protonated, as a result the possibility of nitrogen to be attached on the Au surface will decrease. This might suggest that all the monolayer molecules will be positively charged, which could increase the repulsion among the monolayer molecules and between the positively charged monolayer molecules and the redox probe. Consequently, this will lead to more retardation of the ET reaction compared with 4MP deposited from water.

52

Table 2: Electrochemical parameters obtained from studying the heterogeneous ET reaction by cyclic voltammetry of unmodified and modified gold electrodes.

	ΔE_p (mV)	E_{pa} (mV)	E_{pc} (mV)	E_m (mV)	I_{pc} (mA)	I_{pa} (mA)	D ($cm^2 s^{-1}$)
Bare Au	120	820	700	760	0.54	0.65	3.45×10^{-7}
Au/2MP (H_2O)	847	1126	279	703	0.36	0.36	1.06×10^{-7}
Au/2MP (H_2SO_4)	731	1125	394	760	0.41	0.44	1.58×10^{-7}
Au/4MP (H_2O)	947	1283	336	810	0.36	0.35	1.00×10^{-7}
Au/4MP (H_2SO_4)	1010	1329	319	824	0.37	0.38	1.18×10^{-7}

The results obtained support the conclusion that the gold electrode modified with 2MP and 4MP behaves as a microarray electrode, which allows electron transfer between a redox couple and the electrode surface.

3.2 Electrochemical impedance measurements

The electrochemical impedance measurement (EIM) is a technique that has been used for a long time to study electrochemical processes at the electrode surface. It is a valuable and convenient method to give information on impedance changes of the electrode surface in the modified process. In electrochemical impedance experiments, a small ac voltage is applied to an electrode/solution interface and corresponding electrochemical impedance is obtained. The impedance is measured as a function of the frequency and hence an equivalent circuit can be deduced from the measurements. The components of the equivalent circuit are related to physical features and/or processes at the electrode/solution interface through suitable modeling. However, difficulties in the processing of data using electrical analogs often arise because of the non-linearity in the proposed equivalent circuit.

The impedance is usually composed of real (Z') and imaginary (Z'') part:

$$Z = Z' - j\ Z'' \qquad \text{eq. 6}$$

where $j = (-1)^{1/2}$. There are several ways of plotting the impedance as a function of frequency. The most used one is the Nyquist plot (Z'' *vs* Z' with the frequency as a parameter).

This technique has some advantages as the solution resistance, the double layer capacitance and the current due to diffusion or other processes occurring in the SAMs can be clearly determined [130,132,142]. The results obtained by EIM will be compared with those obtained with cyclic voltammetry.

3.2.1 Electron transfer reaction on a bare gold electrode

Impedance measurements were carried out at the formal potential (E_f) of the redox couple, which was determined from cyclic voltammetry. Fig. 22 shows the impedance measurements of a polycrystalline bare gold electrode in 1.0 **M** aqueous $HClO_4$ solution containing $Fe^{3+/2+}$ redox couple at 0.7 V *vs* RHE, in the frequency range from 0.1 to 10^5 Hz with a value of 5 mV for the amplitude.

As shown in the figure a typical Nyquist diagram is obtained. The impedance-plane plot is characterized by two distinct regions [127,128,132-134,143,144]:

(i) A semicircle in higher frequency region related to charge transfer process. This region is electrically described by a resistance in parallel with a capacitor related to the double-layer. In this region the reaction is purely kinetically controlled.

(ii) A 45° line in the complex-plane impedance plot defining a Warburg region of semi-infinite diffusion of species on the electrode at lower frequencies region. The reaction is in this region diffusion (mass transfer) controlled.
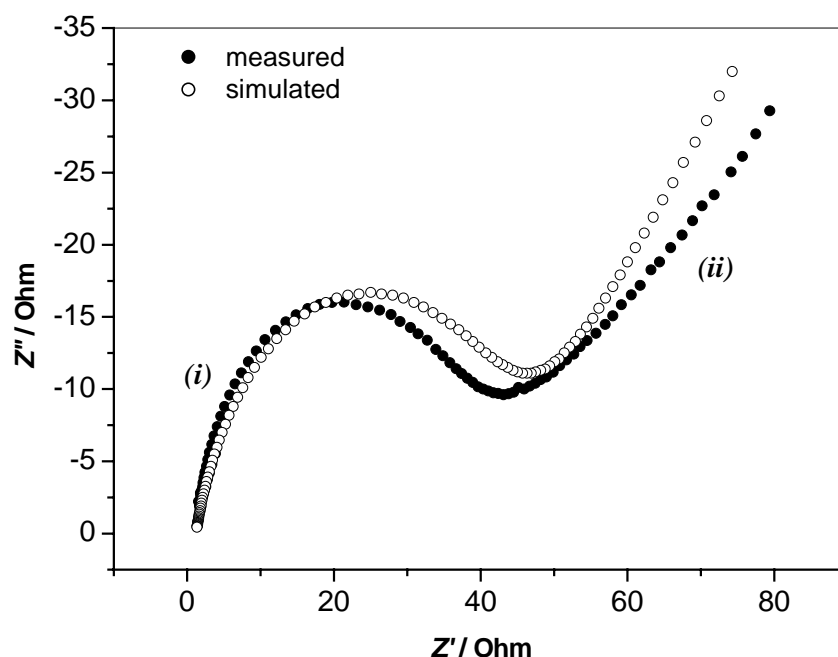
Fig. 22 The measured and the simulated impedance plot of the unmodified gold electrode in the redox solution.

The charge transfer resistance controls the ET kinetics of the redox probe at the electrode surface. It is estimated from the extrapolation of the high-frequency semi-circle to the impedance real axis. The value of the solution resistance is obtained from the impedance data corresponding to the highest frequency [126,144,145].

The circuit model used in this study was a modified Randles circuit that is shown in Fig. 23 where R_s is the solution resistance; R_{ct} is the charge transfer resis-

tance to a species moving through the film, W is the Warburg impedance and C_{dl} is the double layer capacitance [139,146].

$$R_s \quad\quad C_{dl}$$
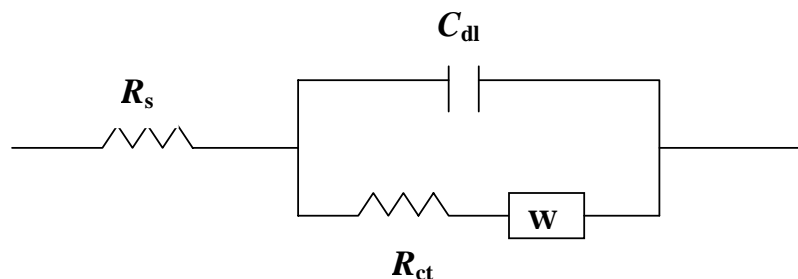
Fig. 23   The proposed equivalent circuit for the bare Au electrode.

The surface changes of the electrode must cause a change in the *ac* response; this change can be understood according to the Randles' equivalent circuit, and can be used to estimate the electrode coverage and the charge transfer rate constant.

A simple equivalent circuit should give a vertical line in the Nyquist plot. However, in many cases, one finds lines with a high but finite slope, and it is also common to find lines with unity slope (corresponding to a phase angle of 45°). This behaviour is represented electrically as a constant phase element (CPE), with an impedance (Z_{CPE}) is given by:

$$Z_{CPE} = 1 \,/\, Q \,(j\,\omega)^{\alpha} \quad\quad \text{eq. 7}$$

where Q is the magnitude of the CPE, $j = (-1)^{1/2}$, $\omega = 2\pi f$ (where f is the frequency of the applied *ac* potential) and α ($0 \leq \alpha \leq 1$) is a parameter that is related to the slope of the Nyquist plot of the Z_{CPE} and determines the behaviour of this element. The experimental value of α is between 0.5 (for an ideally porous electrode) and 1 (for a perfect smooth electrode) [143].

If $\alpha = 1$, the CPE is an ideal capacitor and $Q = C_{dl}$ [142]. A small deviation from 1.0 ($\alpha > 0.80$), as observed here, suggests that the gold substrates are sufficiently smooth for these studies [147]. The charge transfer resistance R_{ct} and the electrode capacitance C_{dl} for $Fe^{3+/2+}$ were calculated using Boukamp software as 5.6 Ω cm^2 and

338.5 µF cm^{-2}, respectively. Higher values of C_{dl} observed are due to high electrochemical active surface [148]

Considering that the electrochemical redox reaction is in equilibrium and the concentrations of the oxidant and reductant are equal, the ET rate constant can be calculated from equation 8 [127,132,126]:

$$k = R \ T \ / \ F^2 \ R_{ct} \ c \qquad \text{eq. 8}$$

where k is the ET rate constant at the Au electrode, R is the gas constant, T is the temperature, F is the Faraday constant and c is the concentration of the redox couple.

The value of the ET rate constant calculated from equation 8 for the bare Au electrode is 4.75×10^{-4} cm s^{-1}. All the obtained parameters characteristic for the bare Au electrode are listed in Table 3 (see page 62).

EIM was used to study the blocking capacity of the formed SAMs, evaluating the presence of defects and/or pinholes in each case, and the obtained results were compared with those obtained by cyclic voltammetry of the redox couple $Fe^{3+/2+}$ at each monolayer.

3.2.2   Influence of 2-mercaptopyridine on the electron transfer reaction

Fig. 24 illustrates the impedance measurements of a Au electrode modified with 2MP deposited from water in 1.0 **M** aqueous $HClO_4$ containing $Fe^{3+/2+}$ redox couple. The same situation as Fig. 22.

When 2MP is deposited from water on Au electrode both the charge transfer and the diffusion processes will be affected. At high frequencies where the electrochemical reaction is purely kinetically controlled the heterogenous charge transfer resistance is increased due to the decrease of the ET rate. At lower frequencies a linear component is present. The Randles equivalent circuit is the same as that of unmodified Au electrode.

The value of the R_{ct} is increased from 5.6 to 380.9 Ω cm^2 while the rate constant is decreased from 4.75×10^{-4} to 6.98×10^{-6} cm s^{-1}. The value of the capacitance is 79.2 μF cm^{-2}. The increase of the charge transfer resistance and the decrease of the rate constant reinforce the conclusion that the SAM may act as a barrier on the electrode surface to the heterogeneous ET reaction [133,134,140]. These results are consistent with those obtained by cyclic voltammetry (Fig. 18).

Fig. 24　Complex impedance plot of Au electrode in the presence of 2MP monolayer deposited from water in 1.0 **M** aqeous HClO$_4$ containing Fe$^{3+/2+}$ redox couple. Same setting as in Fig. 22

The electrode coverage (θ) is a key factor, which can be used to estimate the surface state of the electrode and it is related to the charge transfer resistance. It is assumed that the ET reaction occurs only at bare spots (defects) on the electrode surface and that the diffusion to these defects is planar [133]. According to this assumption, the following equation for the apparent fractional coverage of the electrode can be used [127,128,144]:

58

$$\theta = 1 - (R^\circ_{ct} / R_{ct}) \qquad \text{eq. 9}$$

where R°_{ct} is the charge transfer resistance of the unmodified Au electrode and R_{ct} is the charge transfer resistance of a modified Au electrode.

According to the data obtained from Nyquist plots, a value of $\theta = 0.985$ can be calculated for the Au electrode after immersion in 2MP solution in water. All the obtained electrochemical parameters for the Au electrode modified with 2MP deposited from water are listed in Table 3 (see page 62).

As shown in Fig. 25 when 2MP is deposited from 0.1 **M** H_2SO_4 on the Au electrode a semicircle with a large diameter is obtained followed by a small linear part. This indicates the diminution of the heterogeneous ET reaction that takes place mainly in the kinetically controlled region. The Randles equivalent circuit, which describes this case, is the same as the unmodified Au electrode case.
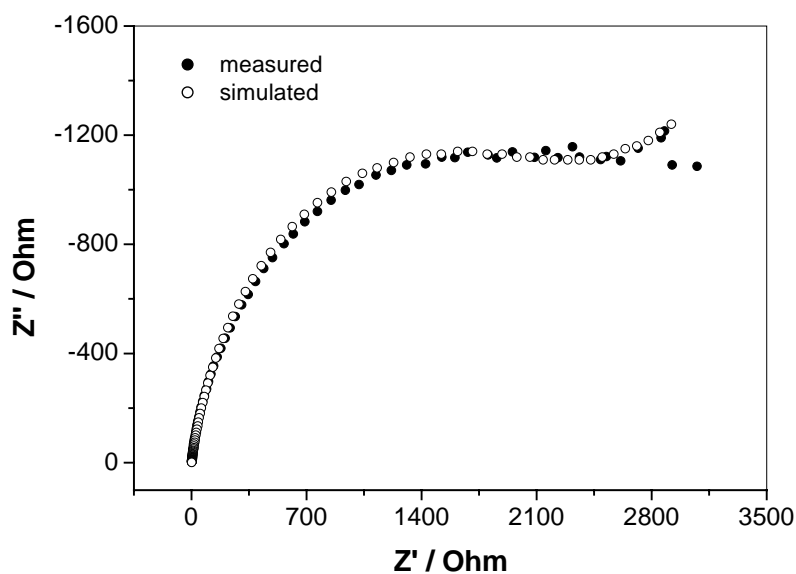
Fig. 25　Complex impedance plot of Au in the presence of 2MP monolayer deposited from 0.1 **M** aqeous H_2SO_4. Same setting as in Fig. 22

From the impedance measurements, the values of R_{ct}, C_{dl}, θ, and of the rate constant are obtained and listed in Table 3 (see page 62). These values encourage the

conclusion that the monolayer hinders the heterogeneous ET process, which is in agreement with the result obtained from cyclic voltammetry (Fig. 19).

On comparing with the case of 2MP deposited from water on the Au surface, it was found that the charge transfer resistance is higher and the rate constant is lower in case of 2MP deposited from water (see Table 3 page 62), which indicates that the approach of the electrochemical species to the electrode surface is facilitated in case of Au electrode modified with 2MP deposited from 0.1 **M** H_2SO_4. The results are consistent with those obtained with cyclic voltammetry (Fig. 18 and 19).

3.2.3 Influence of 4-mercaptopyridine on the electron transfer reaction

Fig. 26 shows the impedance measurements of Au electrode modified with 4MP deposited from water in 1.0 **M** aqueous $HClO_4$ containing $Fe^{3+/2+}$ redox couple. Same circumstances as in Fig. 22.
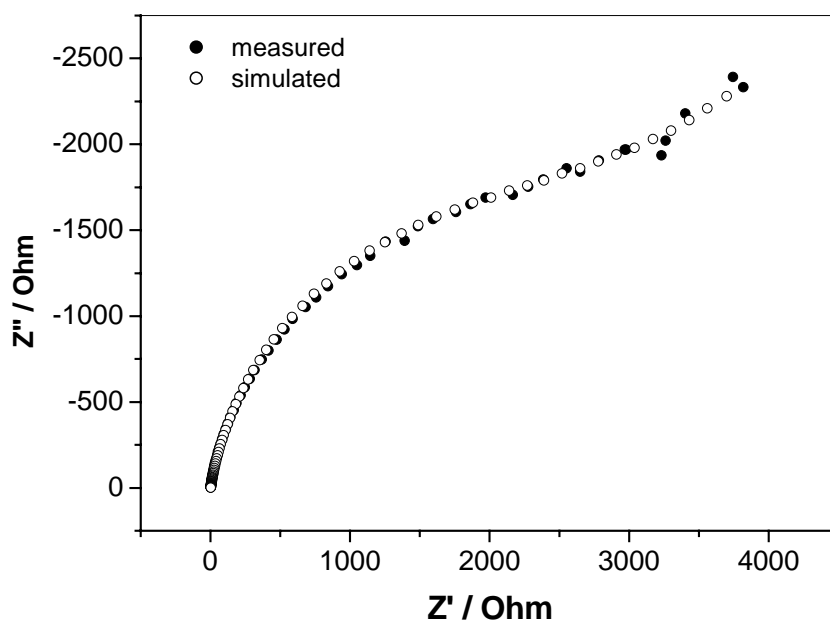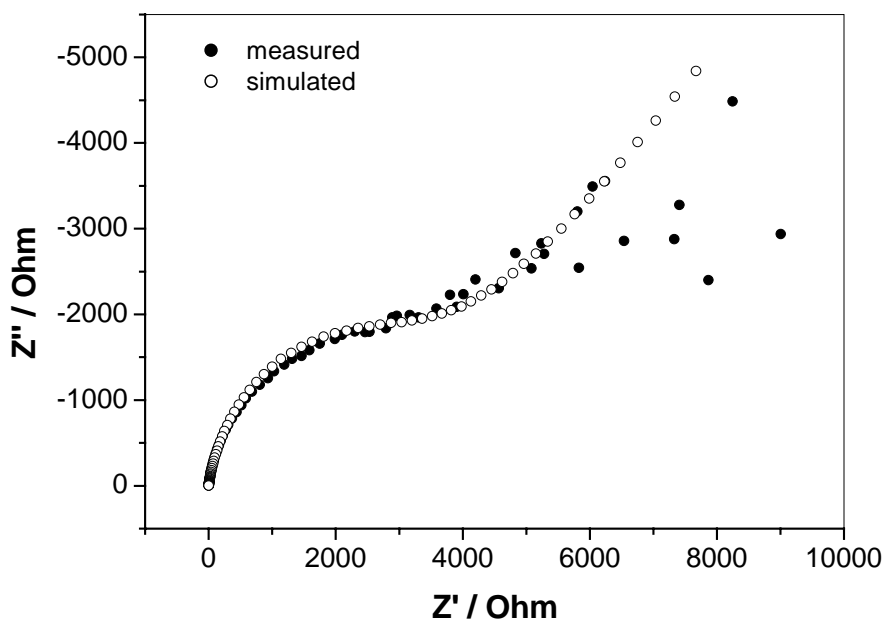

Fig. 26 Complex impedance plot of Au electrode in the presence of 4MP monolayer deposited from water in 1.0 **M** aqueous $HClO_4$ containing $Fe^{3+/2+}$ redox couple. Same circumstances as in Fig. 22.

When 4MP is deposited from water on the Au electrode the Nyquist plot consists of a large diameter semicircle indicating a charge transfer process that became diffusion-controlled process at lower frequencies region. The Randles equivalent circuit of this system is the same as with a bare Au electrode. The obtained values of electrochemical parameters for the Au electrode modified with 4MP deposited from water are listed in Table 3 (see page 62). These values support the cyclic voltammetry results (Fig. 20).

Comparing with 2MP deposited from water on the Au surface, the 4MP monolayer has higher R_{ct} and lower k since the N-atom of the 4MP will be protonated in $HClO_4$ solution, which results in repulsion interaction with the positively charged redox probe and among the monolayer molecules. Also the R_{ct} is higher and the k is lower than in the case of 2MP deposited from 0.1 **M** H_2SO_4 because of the decrease in the density of the active sites in the 4MP monolayer due to the formation of a more compact monolayer. These results are in agreement with those obtained from cyclic voltammetry (Fig. 18-20).

In case of 4MP deposited from 0.1 **M** H_2SO_4 on the Au electrode (Fig. 27) a semicircle showing a higher value for the charge transfer resistance at high frequencies compared with 4MP deposited from water is obtained. The impedance can be modeled by an equivalent circuit as that for unmodified Au electrode or Au electrode modified with monolayers in all other cases.

From the obtained impedance results the values of C_{dl}, θ and k are calculated. On comparison with all the values listed in Table 2, it was found that the resistance is higher for heterogeneous ET process in case of Au electrode modified by 4MP monolayer deposited from 0.1 **M** H_2SO_4. In this case all the N-atoms will be protonated before adsorption, which preclude the adsorption through the N-atom of the pyridine ring so the repulsion interaction is higher in this case than in the case of 4MP in water leading to less ET reaction rate. These results are consistent with those obtained by cyclic voltammetry (Fig. 18-21).
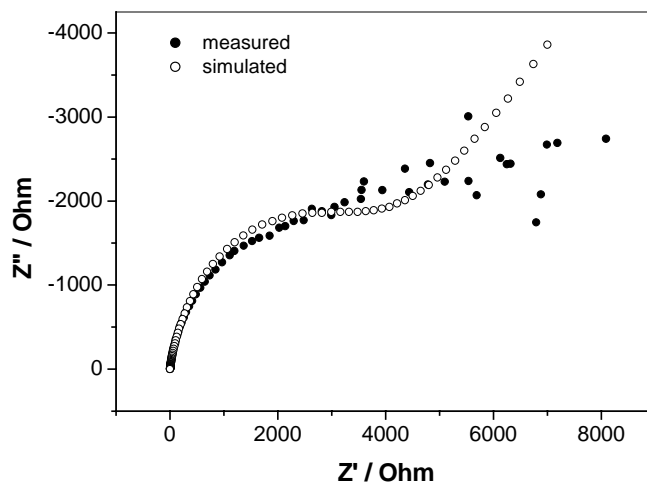
Fig. 27   Complex impedance plot of Au electrode in the presence of 4MP monolayer deposited from 0.1 **M** aqeous H_2SO_4. Same circumstances as in Fig. 22.

Table 3: Electrochemical parameters obtained from impedance measurements for unmodified and modified gold electrodes.

	R_{ct} (Ω cm^2)	C_{dl} (μF cm^{-2})	k (cm s^{-1})	θ
Bare Au	5.6	338.5	4.75×10^{-4}	-
Au/2MP (H_2O)	380.9	79.23	6.98×10^{-6}	0.985
Au/2MP (H_2SO_4)	306.8	69.23	8.67×10^{-6}	0.982
Au/4MP (H_2O)	453.7	72.31	5.86×10^{-6}	0.988
Au/4MP (H_2SO_4)	490.1	83.85	5.43×10^{-6}	0.989

3.3   Surface enhanced Raman spectroscopy

Although electrochemical techniques are suitable for collecting kinetic and thermodynamic data from electrochemical systems, they do not give atomic and molecular scale information on interfacial structures. In order to investigate the correlation between the structure of a self-assembled film and its physical and chemical properties, many surface analytical techniques have been utilized. As a non-destructive sensitive tool for studying the metal-adsorbate interactions and the reactivity of adsorbed species surface enhanced Raman scattering (SERS) is used since it can provide unique information about the structure and the orientation of the molecules adsorbed on the metal surface. Furthermore, several applications of SERS have been written for self-assembled monolayer [149,150], chemical detection [151], biochemistry [152-154] and single molecule detection [155,156].

The most interesting aspect of SERS measurements is the accessibility of a large number of vibrational transitions where modes are associated with specific molecular conformations allowing direct characterization of the structure and the molecular composition [157,158]. Previous research has shown that the frequency of vibrational modes can also yield structural information, where the change in frequency can be correlated with changes in the local environment of the investigated molecule [159,160].

SERS has been widely used in ambient and electrochemical environments [161]. Actually, it is considered to be the most suitable tool for *in situ* observation of surfaces in electrochemical environment. In this work SERS is used to investigate the structure and orientation of self-assembled monolayers.

3.3.1   SER spectra of 4-mercaptopyridine in 0.5 M H_2SO_4

SER spectra of 4-mercaptopyridine, deposited from water on a roughened polycrystalline gold surface, are shown in Fig. 28 at different potentials in 0.5 **M** H_2SO_4. For comparison the Raman spectrum of solid 4MP was also shown in Fig. 29.

When the molecules are chemisorbed on the metal surface, there is an overlapping of the molecular and metal orbitals, the molecular structure will be changed and in the consequence, the positions and relative intensities of SERS bands are dramatically changed [61].
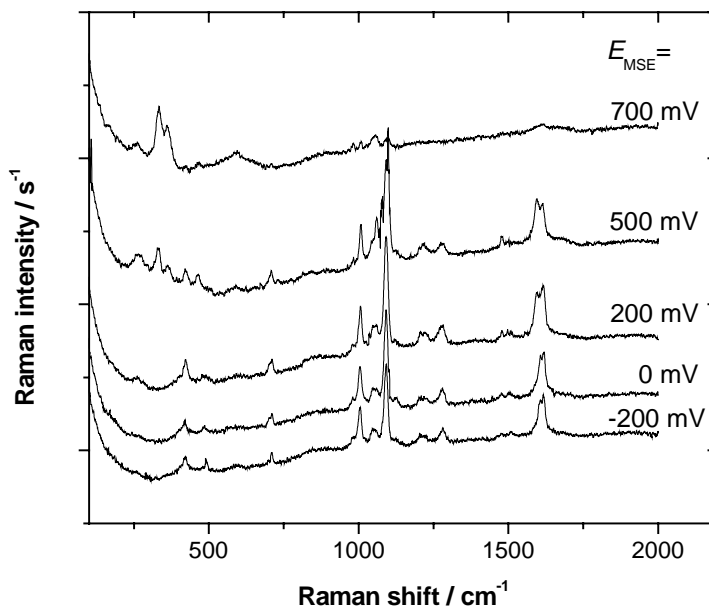
Fig. 28   SER spectra of 4MP deposited from water on a roughened polycrystalline Au electrode in 0.5 **M** H_2SO_4 at different potential values.
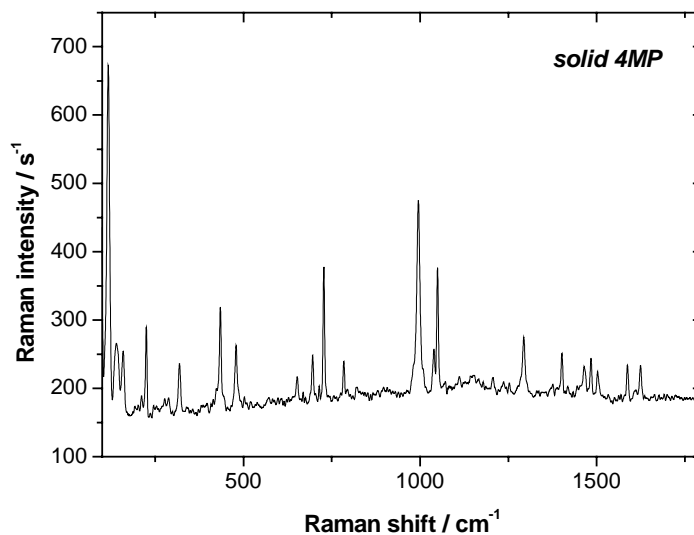
Fig 29   Raman spectrum for solid 4MP.

The frequencies and assignments of Raman bands of solid and adsorbed 4MP are summarized in Table 4. The band assignments are based on Ref. [29,61,162-171].

Table 4: Spectral data of 4MP as a solid and adsorbed from water on a gold electrode, at different electrode potential values.

Wilson #	Symm.	Mode	Solid 4MP	$E_{MSE} =$				
				-200 mV	0 mV	200 mV	500 mV	700 mV
-	-	n.a.	117	-	-	-	-	-
-	-	n.a.	140	-	-	-	-	-
-	-	n.a.	159	-	-	-	-	-
-	-	n.a.	-	-	-	-	-	171
-	-	n.a.	225	-	-	-	-	-
-	-	n.a.	-	-	-	-	-	-
-	-	ν (Au-S)	-	263	263	263	265	265
-	-	$\beta_{i.p.}$ (C-S)	319	-	-	-	-	-
-	-	n.a.	-	-	-	-	330	330
-	-	n.a.	-	-	-	-	364	364
7	a_1	δ (C-S)/γ (CCC)	435	418	418	418	418	418
16	b_1	γ (CCC)	479	488	488	488	-	-
6	b_2	β (CCC)	652	590	-	-	-	590
-	-	n.a.	696	-	-	-	-	-
4	b_1	β (CC)/ ν (CS)	728	711	711	711	711	711
10	b_1	γ (CH)	784	-	-.	-	-	-
-	-	n.a.	-	980	980	979	980	981
1	a_1	ν (ring breathing)	995	1006	1005	1006	1008	1006
18	a_1	$\beta_{i.p.}$ (CH)	1049	1046	1048	1048	1049	1057
18	b_2	$\beta_{i.p.}$ (CH)	1084	-	-	-	-	-
12	a_1	ν (ring breathing)/(C-S)	1111	1092	1092	1092	1093	1095
9	a_1	$\beta_{i.p.}$ (CH)	-	1209	1209	1209	1219	-
3	b_2	$\beta_{i.p}$ (CH)	1293	1281	1280	1280	1274	-
14	b_2	ν (CC)	1402	-	-	-	-	-
19	b_2	ν (C=C/C=N)	1465	1477	1477	1476	1476	-
-	-	n.a.	1484	-	-	-	-	-
-	-	n.a.	1503	1509	1506	1508	1501	-
-	-	n.a.	1587	-	-	-	-	-
8	b_2	ν (C=C)	1611	1607	1607	1607	1595	-
8	a_1	ν (C=C)/(C=N)	1624	1617	1618	1617	1616	1616

ν: stretching; β: bending; $\beta_{i.p.}$: in-plane bending; δ: in-plane deformation; γ: out-of-plane deformation, i.p.: in-plane; n.a.: not assigned.

It is well known that aromatic heterocyclic molecules bearing a mobile H atom undergo rapid and facile tautomeric transformations in solution. It has also been reported that, under ambient conditions, the pyridine derivatives substituted at the 2 or 4 positions by potentially tautomeric groups, SH in this case, exist as the thione tautomer rather than the thiol in polar solution [172]. 4MP is assumed to be present as the thiol-thione tautomer forms (eq.10), in which the thione form is predominant [162,163].

Thiol   *Thione*
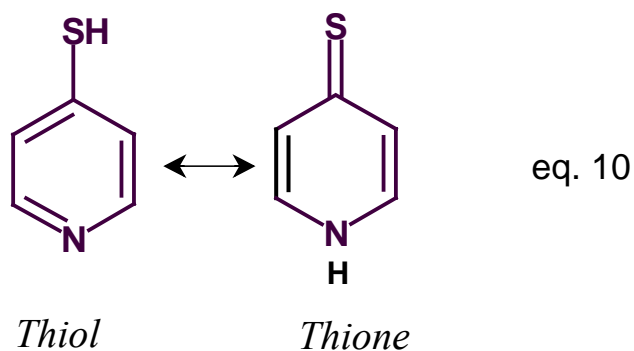
In the set of spectra of <u>Figure 28</u> there is a band at 263 cm^{-1}, which is not appearing in the solid 4MP (<u>Fig. 29</u>). There are some studies of related thiol compounds adsorbed on Au reported by various authors [173-175]. A band at 264 cm^{-1} was assigned by Bron and Holze [61] to the Au-S stretching mode. Joo and coworkers [175] found a Au-S mode with benzyl phenyl sulfide adsorbed on a gold sol at 227 cm^{-1}. In a SER study of adsorbed benzenethiol a mode at 270 cm^{-1} was assigned to a Au-S stretching mode as already proposed previously [176]. Based on these studies the band at 263 cm^{-1} was assigned to be a Au-S stretching mode. This indicates that 4MP is bounded on the Au substrate through the S atom.

All SER spectra of 4MP exhibit a remarkable increase in the intensity of the 12a$_1$ mode near 1092 cm^{-1}. This is a so-called X-sensitive mode [165,166]. X-sensitive modes are described as modes that are strongly coupled substituent and aromatic ring modes such as [ν(ring breathing)/(C-S)]. The local environment of the X substituent modulates the coupling [168]. This coupling has already been noticed in the SERS of thiophenol [166,176], in electrochemical SERS of 4MP on Au electrodes [169] and to a less extent in the normal Raman spectrum of pyridine/metal complexes [176,177]. Another X-sensitive band [β(CC)/ν(C-S)] at 728 cm^{-1} of the solid 4MP

shows a significant downward shift to about 711 cm^{-1} upon the adsorption to the Au surface. Both of these bands are sensitive to the structure and the properties of the substituent. From the preceding discussion it can be judged that 4MP is bonded to the gold surface via the S-atom [166,167,178,179].

Among other changes observed due to adsorption are the downward shift of the ν (C=C)/(C=N) band at 1624 to 1617 cm^{-1}, which was previously reported [161,180,181] as a marker for the N-protonation of 4-mercaptopyridine (4MPH$^+$) as shown in eq. 11.

eq. 11
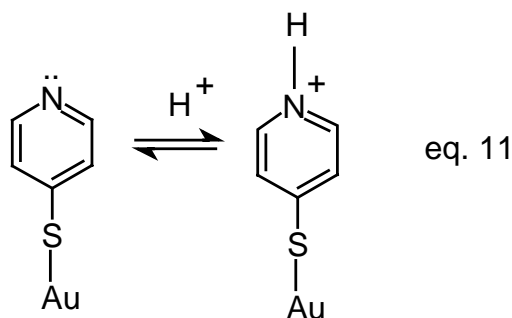
Orientation of the molecule with respect to the electrode surface can be obtained from the shift, appearance and disappearance of bands in surface spectra compared with normal spectra [182-184]. Modes that are perpendicular to the surface are preferentially enhanced. 4MP has C$_{2v}$ symmetry. Thus its vibrational modes can be classified into in-plane a$_1$ and b$_2$ modes and out-of-plane a$_2$ and b$_1$ modes. All these modes are considered as Raman active. For C$_{2v}$ molecules, all four symmetry species are required to define orientation. For perpendicular orientation, the relative enhancement of bands is in the order of b$_1$ = b$_2$ > a$_2$. Molecules which are lying flat on the surface will show enhancements such as a$_2$ = b$_1$ > b$_2$. The a$_1$ totally symmetric vibrational modes cannot be used alone to assign orientation [176]. The b$_1$ modes are weak and a$_2$ modes are not observed at all from 4MP on the SER substrate. The most significant enhancements are appeared for the in-plane ring vibrations as follows 12 a$_1$ ν (ring breathing)/(C-S), 8b$_2$ ν (CC) and 9 a$_1$ β (CH). The inherent weakness of the b$_1$ and absence of the a$_2$ vibrations makes comparison of their relative intensities with those of the a$_1$ and b$_2$ modes impossible [176]. Normal modes that are involved in-plane motion of the ring C=C and C=N bond stretching are expected to be most en-

67

hanced bands which is an indication for more or less perpendicular orientations of molecules with respect to the surface. Out-of-plane a_2 and b_1 vibrations should experience little enhancement. Alternatively, if the molecules were lying flat, the totally symmetric a_1 and non-totally symmetric b_2 in-plane vibrations would experience little or no enhancement. Some out-of-plane vibrations would be enhanced. In the SER spectra of 4MP, the $1a_1$ in-plane totally symmetric ring vibration appears as an intense band. Preferential enhancement of the in-plane $12a_1$, $9a_1$, and $8b_2$ vibrations suggests that the plane of the pyridine moiety is roughly perpendicular to the surface.

Fig. 28 shows the SER spectra of 4MP at different applied potentials. The specta were recorded only with a potential window between oxidation and reduction (from – 200 to 700 mV *vs* MSE) to avoid contributions from reduction/oxidation products. As described above there will be some differences in the peak positions and band intensities due to adsorption.

There are major changes can be observed in the SER spectra with different potentials. First, in the low frequency region the intensity of the band at 263 cm^{-1}, which was assigned to Au-S stretching, was found to be very weak at potentials from – 200 to 0 mV *vs* MSE. Then its intensity increased with increasing potential. The lower intensity of this band may be attributed to the protonation of the N-atom in acidic medium that results in a weakening of the Au-S bond, as mentioned before, and then the interaction of Au-S became stronger as the potential is increased. Second observation is the upward shift from 1092 to 1095 cm^{-1} and the increasing of the intensity of the 12 a_1 ν (ring breating)/(C-S) band with the increasing of the potential. Similar ν (C-S) peak shift and enhancement have been observed for thiopental adsorbed via the S-atom on SERS-active metal substrates [166,185]. A third change is the increasing of the intensities of the band 19 b_2 ν (C=C)/(C=N) at 1477 cm^{-1} and the band 4 b_1 β (CC)/ ν (CS) at 711 cm^{-1}. In addition the 8 b_2 ν (C=C) band was shifted from 1607 to 1595 cm^{-1}. At potentials – 200, 0 and 200 mV *vs* MSE the $8a_1 \nu$ (CC) band at 1616 cm^{-1} is stronger than that at nearly 1607 cm^{-1}. At 500 mV, several new bands appear at 330, 364 and a broad band at 590 cm^{-1}. A completely different spectrum is obtained at 700 mV. At this potential the oxidation of the 4MP is started as can be seen from the cyclic voltammetry results (see Fig. 8). Since the major changes of the SER spectra with increasing the potential are obtained for the bands which are related to S-atoms,

it can be concluded that 4MP molecules deposited from water on Au surface might be adsorbed through the S-atom. It was published that 4MP molecules could bind to the surface through N-atom [64,67]. Nevertheless the obtained SER spectra (Fig. 28) do not show evidence of the Au-N bond.

4MP deposited from 0.5 M H_2SO_4:

Fig.30 represents the set of SER spectra for 4MP deposited from 0.1 **M** aqueous H_2SO_4 on a Au surface. The details of band positions and their assignment are collected in Table 5.
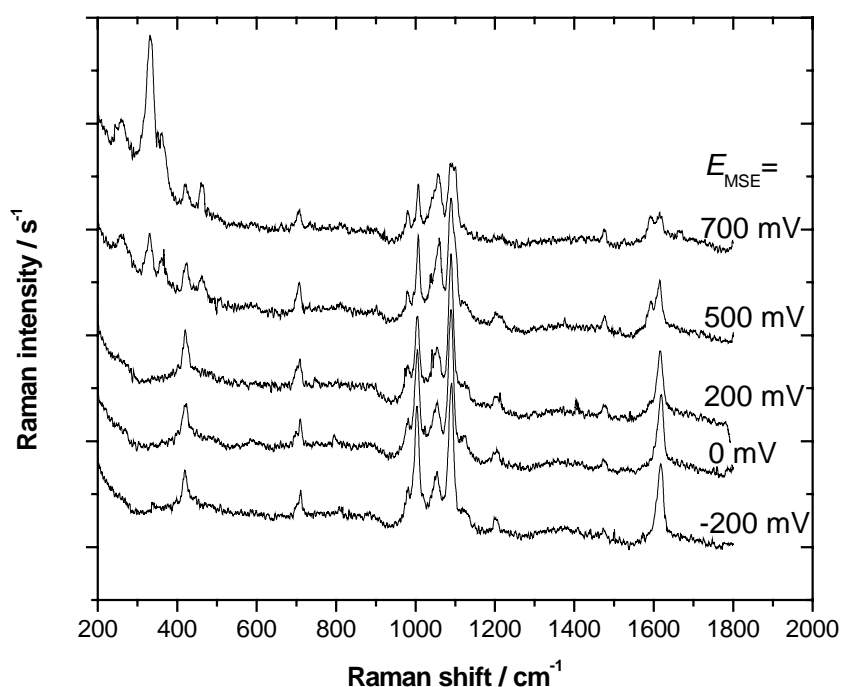
Fig. 30 SER spectra of 4MP deposited from 0.1 **M** H_2SO_4 on a roughened polycrystalline Au electrode at different potential values in 0.5 **M** H_2SO_4.

In Fig. 30 a band around 260 cm^{-1}, that was assigned to Au-S stretching, was observed. In addition, an increase of the intensity of the X-sensitive band at 1090 cm^{-1} and a shift of another X-sensitive band from 728 cm^{-1} of the solid 4MP to 711 cm^{-1} can be observed upon adsorption on the Au surface. The appearance of the band at 260 cm^{-1}, the increase of the intensity of the band at 1090 cm^{-1} and the downward

shift of the band at 728 cm^{-1} are evidence for the adsorption of 4MP monolayer through the S-atom on the gold surface.

Table 5: Assignments and wavenumber positions (cm^{-1}) for normal Raman and SERS of 4MP deposited from 0.5 **M** H$_2$SO$_4$ on Au electrode [29,61,162-171].

Wilson #	Symm.	Mode	Solid 4MP	$E_{MSE} =$				
				-200 mV	0 mV	200 mV	500 mV	700 mV
-	-	n.a.	117	-	-	-	-	-
-	-	n.a.	140	-	-	-	-	-
-	-	n.a.	159	-	-	-	-	-
-	-	ν (Au-S)	-	260	260	260	258	258
-	-	$\beta_{i.p.}$ (C-S)	319	-	-	-	-	-
-	-	n.a.	-	337	-	-	330	331
-	-	n.a.	-	-	-	-	363	359
7	a$_1$	δ (C-S)/ γ (CCC)	435	419	422	419	422	419
-	-	n.a.	-	-	-	-	459	460
16	b$_1$	γ (CCC)	479	-	-	-	-	-
6	b$_2$	β (CCC)	652	-	-	-	-	-
-	-	n.a.	696	-	-	-	-	-
6	a$_1$	β (CC)/ δ (C=S)	728	711	710	711	707	707
10	b$_1$	γ (CH)	784	-	-	-	-	-
-	-	n.a.	-	809	795	-	-	-
-	-	n.a.	-	982	982	978	987	979
1	a$_1$	ring breathing	955	1003	1003	1001	1007	1007
18	a$_1$	β (CH)	1049	1054	1053	1054	1069	1056
18	b$_2$	β (CH)	1090	1090	1089	1092	1090	1087
12	a$_1$	ring breathing/ (C-S)	1111	1124	1126	1122	-	-
9	a$_1$	β (CH)	-	1198	1205	1203	1209	-
-	-	n.a.	1293	-	-	-	-	-
14	b$_2$	ν (CC)	1402	-	-	1405	1375	-
19	b$_2$	ν (C=C)/(C=N)	1465	1472	1472	1477	1476	1478
19	a$_1$	n.a.	1484	-	-	-	-	-
-	-	n.a.	1503	-	-	-	-	-
-	-	n.a.	1587	-	-	-	1591	1591
8	b$_2$	ν (C=C)	1611	-	-	-	-	-
8	a$_1$	ν (C=C)/(C=N)	1624	1617	1619	1613	1617	1614

ν: stretching; β: bending; $\beta_{i.p.}$: in-plane bending; δ: in-plane deformation; γ: out-of-plane deformation, i.p.: in-plane; n.a.: not assigned

The SER spectra at increasing potential values show a dramatical enhancement of the bands at 260, 711, 1090 and at 1472 cm^{-1}. Another observation is the increase of the intensity of the band at 1617 cm^{-1}, which is related to 8 a$_1$ ν (CC). The latter band will split at 500 mV *vs* MSE into two bands at 1591 and 1617 cm^{-1}. New bands can be achieved at 330, 363 and 459 cm^{-1} at 500 mV. The oxidation of the 4MP monolayer is started at 700 mV.

Comparing with SER spectra of 4MP deposited from water (Fig. 28) the bands at 1503 and 1293 cm^{-1} (of the solid 4MP) are disappeared and the others at 1054, 711 and 419 cm^{-1} became more stronger in case of 4MP deposited from acid. It can be concluded that the change of the SER spectra can be observed mainly for the X-sensitive bands in case of 4MP deposited from H$_2$SO$_4$. This suggests that the possibility of adsorption of 4MP might be only via S-atom since the N-atoms of 4MP are protonated in the acidic solvent.

3.3.2 SER spectra of 2-mercaptopyridine in 0.5 M H$_2$SO$_4$

Fig. 31 presents the results of SER spectra of 2MP deposited from water on a roughened polycrystalline gold surface at different potentials in 0.5 **M** aqueous H$_2$SO$_4$. For comparison the Raman spectrum of solid 2MP was also shown in Fig. 32 (see page 73).

Significant differences between these two classes of spectra can be seen indicating that the molecules show a structural change due to adsorption on the metal surface. The peak position and band assignments are summarized in Table 6 (see page 74). The bands assigned according to Ref. [162,163,186,187].

It is known that 2MP exists in the solid state in its thione form as a hydrogen-bonded dimer (eq. 12) [188,189]. However, when 2MP is adsorbed onto the metal surface through the sulfur group, such hydrogen-bonded dimers cannot be formed, hence the molecules should adopt a configuration more like that of a thiol form.

eq. 12
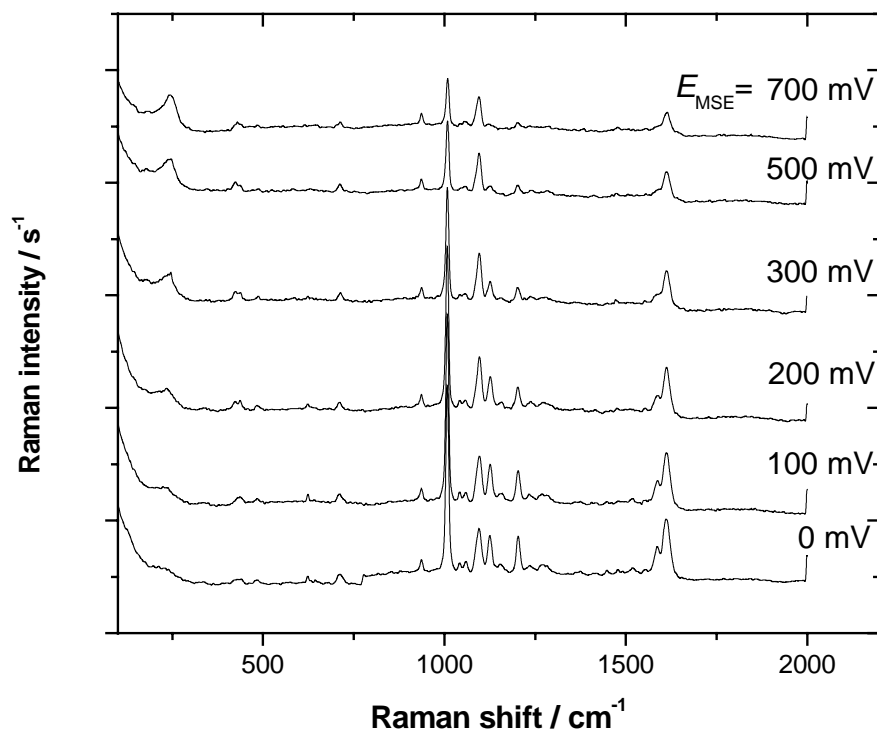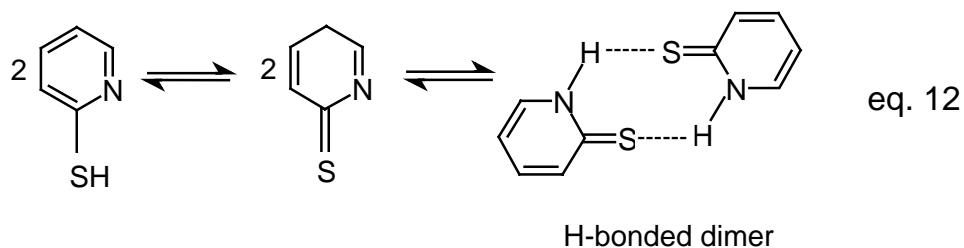
Fig. 31 SER spectra of 2MP deposited from water on a roughened Au electrode at different potential values in 0.5 **M** aqueous H_2SO_4.

Comparing the spectra of solid 2MP with the adsorbed on the metal surface shows that the thione form is predominant when the molecules are in the solid state, but the thiol-like form is observed for molecules adsorbed on the gold surface. This comparison shows substancial differences in the case of the thiol. Many bands that are strong in the solid spectrum are not observed or are extremely weak in the surface spectra. In addition, many bands undergo significant frequency shifts. The loss of the proton and formation of an Au-S bond may account for some of the differences.
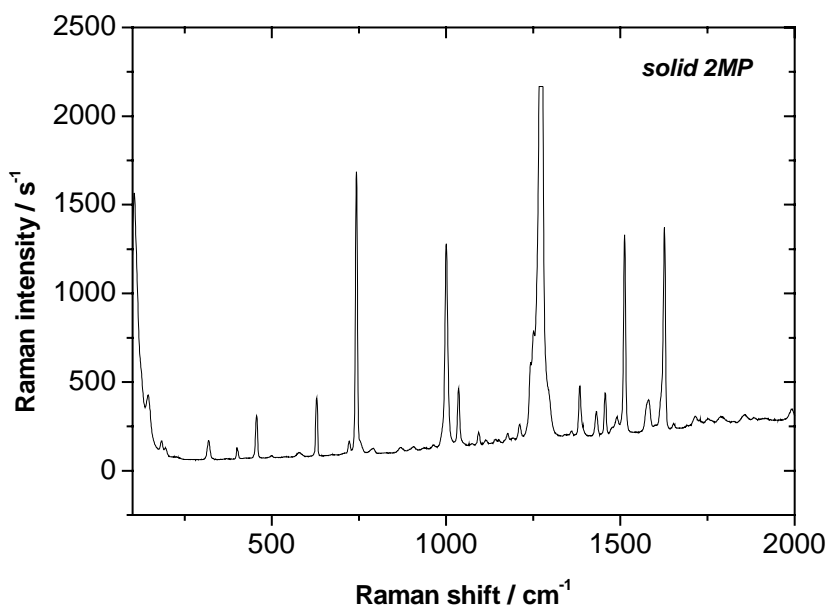
Fig 32 Raman spectrum of solid 2MP

In the SER spectra of 2MP (Fig. 31) there is a band at 235 cm^{-1}, which does not appear in solid 2MP (Fig. 32). Based on previous studies [61,173-175] this band was assigned to Au-S stretching mode. This indicates that 2MP is bounded on the Au substrate through the S-atom. The ring modes containing CS stretching vibration such as 6 a$_2$ ν (CS) and 6 a$_1$ ν (CS), which appear at 456 and 722 cm^{-1} respectively in the solid 2MP are red shifted to 430 and 712 cm^{-1} in the SER spectrum. This is another indication of the involvement of the S-atom in the adsorption process. Another X-sensitive band at 1113 cm^{-1} is blue shifted to 1125 cm^{-1} and its intensity will increase. [166,176,179,190].

There are three bands related to the N-atom. The first band [19 a ν (C=C/C=N)] is shifted from 1512 cm^{-1} to 1519 cm^{-1} due to adsorption. The second band, which is found at 1456 cm^{-1} [19 b ν (C=C/C=N)] in the Raman spectrum of the solid 2MP is shifted to 1448 cm^{-1} with a lower intensity in the SER spectra of 2MP. A third one is the high intensity sharp band [14 b ν (C=C/C=N)] at 1273 cm^{-1} became a very weak broad band. These results suggest that the N-atom of the 2MP molecule interact with Au surface forming the chelate structure (Fig. 6).

Table 6: A comparison of normal Raman and SERS of 2MP, deposited from water, on a roughened Au surface at different potentials [61,166,173-176,179,190].

Wilson#	Symm.	Mode	Solid 2MP	$E_{MSE} =$					
				0 mV	100 mV	200 mV	300 mV	500 mV	700 mV
-	-	n.a	145	-	-	-	-	-	-
-	-	n.a.	184	-	-	182	182	181	181
-	-	ν (Au-S)	-	235	236	238	238	243	242
-	-	β (CS)	340	-	-	-	-	-	-
6	a	δ (C-S) / γ (CCC)	456	430	432	429	429	428	428
-	-	n.a.	-	484	483	479	485	-	-
-	-	n.a.	577	-	-	-	-	-	-
6	a	γ (CCC)	629	623	623	625	-	-	-
-	-	ν (CS)	722	712	712	709	715	714	714
-	-	n.a.	743	-	-	-	-	-	-
-	-	n.a.	789	-	-	-	-	-	-
-	-	n.a.	-	937	937	932	938	938	938
1	a	ring breathing	1000	1010	1010	1006	1008	1008	1010
18	a	β (CH)	1036	1042	1045	1043	1041	-	-
-	-	n.a.	-	1059	1056	1054	1052	1054	1054
18	b	β (CH)	1093	1093	1093	1095	1095	1093	1094
12	a	ring breathing / ν (C-S)	1113	1125	1129	1129	1125	1125	1127
-	-	n.a.	1176	1154	1157	1157	1153	-	-
-	-	n.a.	1211	1203	1207	1202	1202	1203	1203
-	-	n.a.	-	1235	1235	1235	1239	1239	-
14	b	ν (C=C/C=N)	1275	1273	1275	-	-	-	-
-	-	γ (CH)	1384	-	-	-	-	-	-
-	-	n.a.	1432	-	-	-	-	-	-
19	b	ν (C=C/C=N)	1456	1448	1448	-	-	-	-
-	-	n.a.	1491	-	-	-	-	-	-
19	a	ν (C=C/C=N)	1512	1519	1519	-	-	-	-
8	b	ν (C=C)	1579	1586	1583	1583	1575	1575	-
8	a	ν (C=C)	1626	1610	1610	1610	1609	1608	1608

ν: stretching; β: bending; δ: in-plane deformation; γ: out-of-plane deformation, i.p.: in-plane; n.a.: not assigned

In addition, bands at 1036 and 1000 cm^{-1} arise from β (CH) and ring breathing display characteristic spectra shift to 1042 and 1010 cm^{-1} respectively due to adsorption. Other bands at 1626 and 629 cm^{-1} due to 18 ν (CC) and γ (CCC) are red shifted to 1610 and 623 cm^{-1} respectively. New bands at 1235, 1059 and 484 cm^{-1} appear while the assignments at 1432, 1384, and 789 cm^{-1} disappear from the SER spectra.

It is assumed that the 2MP molecule retains its original *Cs* symmetry in the normal Raman spectrum. 2MP probably binds also with a predominantly perpendicular orientation to the Au surface [162,163].

The SER spectra of 2MP (Fig. 31) were recorded in the potential range between oxidation and reduction (from 0 to 700 mV *vs* MSE) to avoid contributions from oxidation/reduction products. Remarkable differences can be observed with different potentials. The first change that can be noticed in the SER spectra is the increasing of the intensity of the ν (Au-S) band at 231 cm^{-1} with increasing the potential. Different from 4MP, this band is clearly appearing in the spectra starting from 0 mV. This suggests the idea that 2MP adsorbed more strongly on the Au surface than 4MP owing to the formation of the chelate ring through S- and N-atoms as has been previously concluded from the cyclic voltammetry measurements. Second observation is the increase of the intensity of the X-sensitive band at around 430 cm^{-1} as the potential increase. The third change is the decrease of the intensities of the bands at 1042 and 1059 cm^{-1}. The latter band is downshifted to 1054 cm^{-1} with increasing the potential. Nearly all the intensities of the other bands in the spectra decreased.

Compared with 4MP (Fig. 28), the spectrum of 2MP at 700 mV shows that the monolayer is still stable on the Au surface, which is not the case of 4MP. This might suggest that 2MP binds to the Au surface stronger than 4MP and the 2MP monolayer is more stable than 4MP monolayer with different potentials.

2MP deposited from 0.1 M H$_2$SO$_4$:

The SER spectra of 2MP deposited from 0.1 **M** H$_2$SO$_4$ on Au substrate are shown in (Fig. 33). The assignments of the bands are collected in Table 7 (see page 77).

In Fig. 33, the band arises from Au-S stretching can be detected at 215 cm^{-1} and it is up shifted with increasing the potential to the value of 220 cm^{-1} at 700 mV *vs* MSE. The X-sensitive bands at 456, 722 and 1113 cm^{-1} of the solid state are shifted to 434, 715 and 1119 cm^{-1}, which present another evidence for the adsorption of 2MP via S-atom on the substrate.
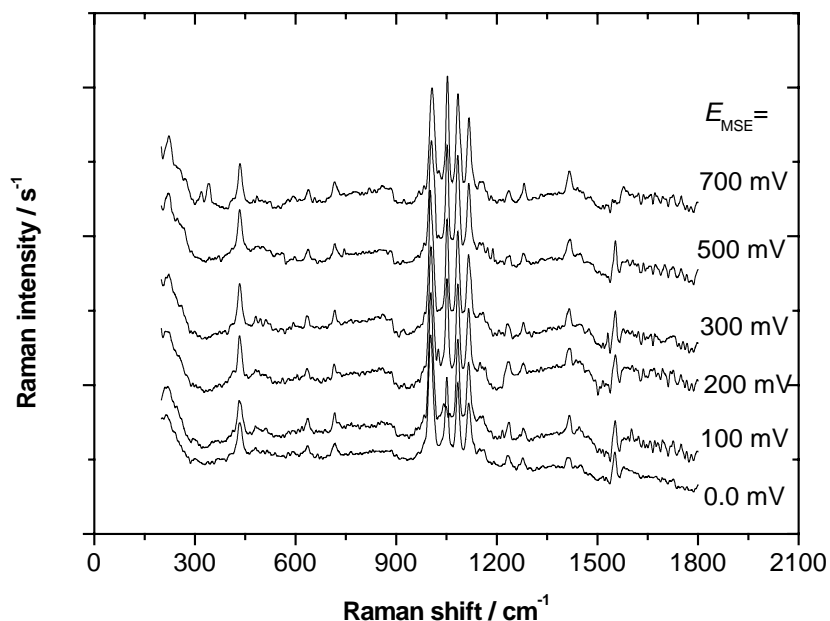
Fig. 33 SER spectra of 2MP deposited from 0.1 **M** H_2SO_4 on a roughened polycrys-
talline Au substrate in 0.5 **M** aqueous H_2SO_4 at different potentials.

The intensity of the (14 b ν (C=C/C=N) band at 1275 cm^{-1} is decreased in the SER spectra of 2MP and it is shifted to 1281 cm^{-1}. Also the 19 b ν (C=C/C=N) band at 1456 cm^{-1} is shifted to 1446 cm^{-1}. The band near 1230 cm^{-1} in the SER spectra may be related to the coupled mode β (CH)/δ (NH). These may be evidences for the protonated N-atom in the acidic solvent [162].

In addition, the β (CH) bands at 1036 and 1093 cm^{-1} in the solid 2MP are shifted to 1052 and 1082 cm^{-1} and their intensities are increased remarkably upon adsorption. The ν(C=C) band at 1626 cm^{-1} disappeared from the SER spectra. Also new bands appeared at 263 and 1548 cm^{-1}. Others at 319 and 345 cm^{-1} are noticed at 700 mV *vs* MSE.

76

Table 7 Spectra data and vibrational assignments for normal Raman and SERS of 2MP deposited from 0.1 **M** H_2SO_4 on Au substrate at different potentials [61,166,173-176,179,190].

Wilson#	Symm.	Mode	Solid 2MP	$E_{MSE} =$					
				0 mV	100 mV	200 mV	300 mV	500 mV	700 mV
-	-	n.a.	145	-	-	-	-	-	-
-	-	n.a.	184	-	-	-	-	-	-
-	-	ν(Au-S)	-	215	217	217	223	220	220
-	-	n.a.	-	-	-	263	263	263	263
-	-	β(CS)	-	-	-	-	-	-	319
-	-	n.a.	340	-	-	-	-	-	345
-	-	δ(C-S)/ β(CCC)	456	434	436	430	435	434	433
-	-	n.a.	-	481	482	482	482	482	484
-	-	n.a.	-	-	513	-	512	506	-
-	-	n.a.	577	-	-	559	-	562	593
6	a	γ(CCC)	629	637	639	633	631	633	641
-	-	ν(C-S)	722	715	716	711	720	718	719
-	-	n.a.	743	-	-	-	-	-	-
-	-	n.a.	-	888	839	887	891	898	890
1	a	(ring breathing)	1000	1005	1002	1002	1003	1007	1004
18	a	β(CH)	1036	1052	1048	1051	1055	1055	1055
18	b	β(CH)	1093	1082	1082	1082	1082	1081	1088
12	a	ring breathing/ν(C-S)	1113	1119	1115	1116	1119	1118	1119
-	-	n.a.	1176	1159	1157	1160	1160	1150	1155
-	-	n.a.	1211	-	-	-	-	-	-
-	-	β(CH)/ δ(NH)	-	1236	1236	1233	1233	1237	1238
14	b	ν(C=C)/(C=N)	1275	1278	1278	1279	1280	1281	1281
-	-	γ(CH)	1384	1382	-	-	-	-	-
-	-	n.a.	1432	1418	1418	1413	1413	1419	1416
19	b	ν(C=C)/(C=N)	1456	1455	1430	1446	1447	1450	1446
19	a	n.a.	1491	1472	1474	1477	1477	1481	
-	-	n.a.	1512	1516	-	1516	1529	-	1526
8	b	n.a.	-	1548	1553	1555	1555	1555	-
8	b	ν(C=C)	1580	1579	-	-	-	1574	1578
8	a	ν(C=C)	1626	-	-	-	-	-	-

ν: stretching; β: bending; δ: in-plane deformation; γ: out-of-plane deformation, i.p.: in-plane; n.a.: not assigned.

For comparison between 2MP deposited from water and from H_2SO_4 <u>Fig. 34</u> shows the SER spectra for both cases at 300 mV *vs* MSE.
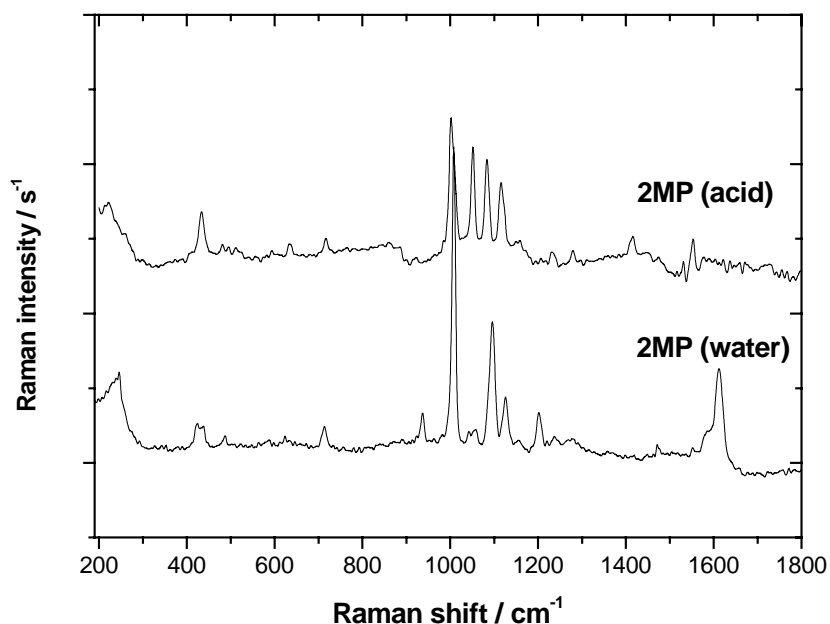

Fig. 34 SER spectra of 2MP deposited on Au electrode at 300 mV *vs* MSE.

Significant differences can be noticed between the two spectra. First, the Au-S stretching appeared at 235 cm^{-1} in case of 2MP deposited from water and at 215 cm^{-1} in case of 2MP deposited from acid. Then, the X-sensitive band around 430 cm^{-1} is more sharp and intense for the latter case. The other X-sensitive bands appeared at 712 and 1124 cm^{-1} for deposition from water and at 717 and 1119 cm^{-1} for deposition from acid. The third difference is the 18 a β (CH) band at 1052 cm^{-1} in case of acidic solvent is more intense than that in case of water, which appears as a broad weak band at around 1045 -1060 cm^{-1}. The ring-breathing mode at 1203 cm^{-1} in case of deposition from water has higher intensity than that of the acidic solvent. There is a band at 1553 cm^{-1} in case of 2MP adsorbed from acid, which does not exist in the case of water and the ν (C=C) band at 1609 cm^{-1} exists only for 2MP adsorbed from water. These changes may be due to the formed chelate ring when 2MP is deposited on Au surface from water, which does not exist in the case of acidic solvent since the N-atom is protonated.

78

3.4 Corrosion inhibition

Corrosion in pipes, pumps, turbine blades, coolers, superheaters, reheaters, fuel cells, and exhaust systems causes enormous industrial expense due to production downtime, accidental injuries, and replacement costs [191]. Steel is an important metal in industrial applications, but it can be easily oxidized in air. The chloride ions significantly promote the corrosion process in aqueous solution, such as seawater. In recent years, SAMs have offered a method to diminish corrosion of the metals. One of the most important methods in corrosion protection of metals is the use of organic inhibitors to protect the metal surface from the corrosive environments. The inhibition efficiency of the organic compounds is closely related to the structure and the properties of the film formed on the metal surface [192,193].

In order to study the inhibition of the SAMs in the selected medium, a number of methods can be used. Among the rapid methods of detection, the electrochemical impedance measurement is one of the most valuable methods. Generally, equivalent circuits are used to interpret the electrochemical impedance values obtained for inhibitors performance in corrosion studies [194-206].

3.4.1 Study of the corrosion of C60 steel electrode by EIM

In the electrochemical experiment, the iron will be dissociated on the anode according to equation 13 [207] as follows

$$\text{Anode: } Fe = Fe^{2+} + 2e^- \qquad \text{eq. 13}$$
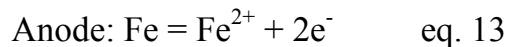
This reaction is rapid in most media [207]. The cathodic reaction is given by equation 14. This reaction proceeds rapidly in acids but only slowly in alkaline or neutral media

$$\text{Cathode: } 2H^+ + 2e^- = H_2 \qquad \text{eq. 14}$$
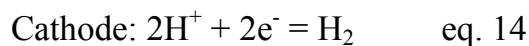
The cathodic reaction in neutral and alkaline media is accelerated by dissolved oxygen in accord with the depolarization reaction equation 15

$$\tfrac{1}{2}\,O_2 + H_2O + 2e^- = 2OH^- \qquad \text{eq. 15}$$
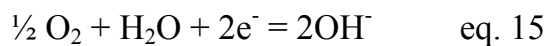
The Nyquist plot of C60 steel electrode in 3.5% aqueous NaCl solution at -0.57 V *vs* SCE with 5 mV amplitude is presented in Fig. 35. The frequency range is 0.1 – 10^5 Hz.
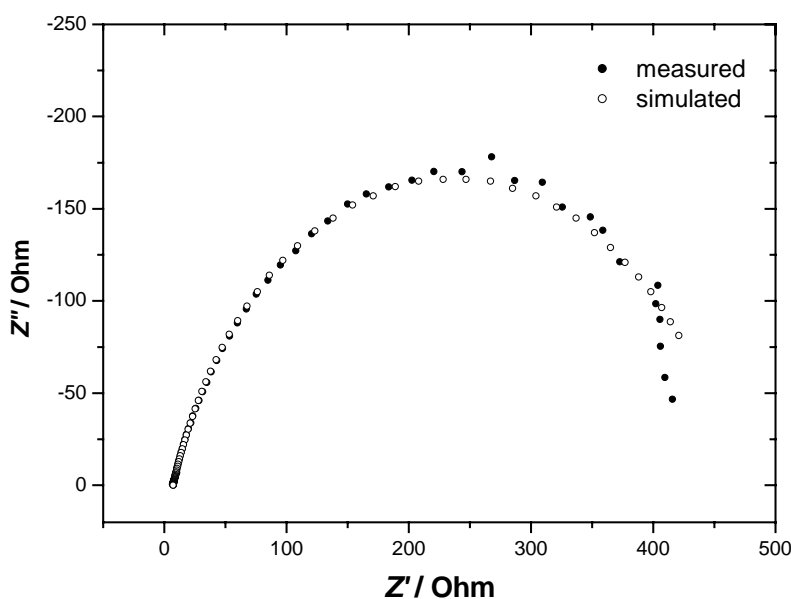
Fig. 35   The measured and the simulated Nyquist plot of EIS of C60 steel electrode.

The polarization (or the charge transfer) resistance R_p value of the steel electrode is obtained by calculating the semicircle intersection via curve fitting of impedance data using Boukamp software. The value of R_p was found to be equal to 459 Ω.

The influence of 2MP and 4MP on the corrosion of the steel electrode was studied after immersion of the electrode for 3 minutes in the aqueous solution of the mercaptopyridines.

3.4.2 Influence of 2-mercaptopyridine on the corrosion of C60 steel electrode

Fig. 36 shows the complex plane of the resulting impedance data for C60 steel electrode in the presence and in the absence of 2MP monolayer. The conditions are the same as for the bare steel electrode.

Fig. 36 Nyquist impedance plots of steel electrode in presence and absence of 2MP monolayer in 3.5% NaCl

It is clear that the presence of 2MP monolayer produced a higher R_p value, which is an indication of the formation of an effective protective film that hindered corrosion. The inhibition efficiency (η %) was determined using the following formula [208]:

$$\eta \, (\%) = (1 - R_p^\circ / R_p^{inh}) \, 100 \qquad \text{eq. 16}$$

where R_p° and R_p represent the electrode polarization resistance in the absence and the presence of the inhibitor, respectively. The polarization resistances and the inhibition efficiency results are collected in Table 8 (see page 82).

3.4.3 Influence of 4-mercaptopyridine on the corrosion of C60 electrode

Fig. 37 shows the complex plane of the impedance data for C60 steel electrode in the presence and in the absence of 4MP monolayer. The conditions are similar as the bare steel electrode.
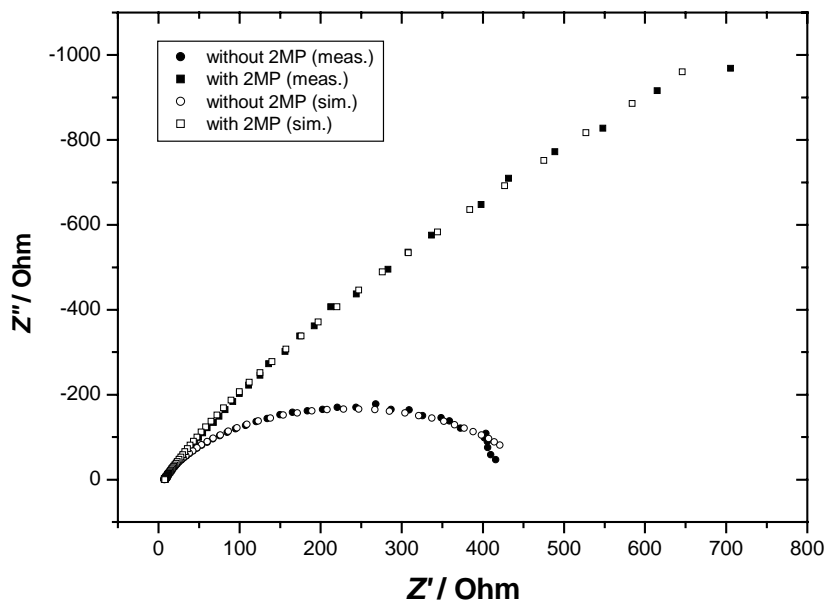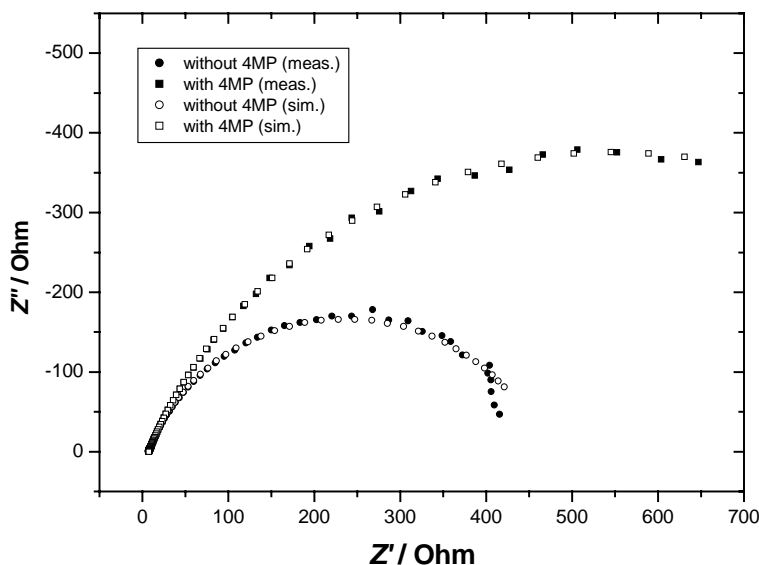

Fig. 37 Nyquist impedance diagrams of steel electrode in presence and absence of 4MP monolayer in 3.5 % NaCl

As can be seen from the figure the presence of 4MP monolayer shows a higher polarization resistance value than a bare electrode, which indicates that 4MP can serve as corrosion inhibitor for steel in NaCl solution. However, 4MP exhibits less inhibition efficiency than 2MP, which might be due to the presence of a chelate structure in 2MP.

Table 8 EIS (R_p and η) results for steel electrode in the absence and presence of the monolayer

	R_p / Ω	η (%)
Bare Fe	459	-
2MP	1.25×10^3	75
4MP	1.08×10^3	58

These results encourage further studies for the mercaptopyridines at different conditions to select the best inhibition efficiency for steel electrode and other electrodes in different electrolyte solutions.

Summary

Formation and subsequent characterization of self-assembled monolayers (SAMs) have become important in the field of chemical research today as self-assembly is a versatile technique for surface modification for different applications. Thiol monolayer on Au has received considerable attention due to its simplicity and ease of preparation. The formation of SAMs of 2- and 4-mercaptopyridines on the surface of the polycrystalline gold electrode deposited from either water or aqueous 0.1 **M** H_2SO_4 has been successfully carried out. The behaviour of these monolayers was also studied in different electrolytic media. Overview about self-assembled monolayers and the experimental methods used in the investigations are mentioned clearly. It is also worthy to say that mercaptopyridines were.

The results obtained by cyclic voltammetry technique, electrochemical imped-ance measurements (EIM) and surface enhanced Raman spectroscopy (SERS) have been intensively interpreted. The oxidation and reduction potentials of the SAMs of 2-mercaptopyridine (2MP) and 4-mercaptopyridine (4MP) on gold surface in 0.5 **M** aqueous H_2SO_4 are obtained and discussed in detail. 2MP deposited from water is suggested to be adsorbed on the surface through the formation of S-Au-N chelate, whereas 4MP has the possibility to adsorb through S-atom (normal geometry). Ac-cordingly, 2MP is more strongly adsorbed on the Au electrode than 4MP. It is prob-able that 4MP is also bonded to the gold electrode through the N-atom (out of normal geometry). In the acidic solvent, 2MP and 4MP will be attached only through the S-atom to the surface since the N-atom is protonated in the acidic solvent.

The electrochemical deposition of copper is investigated using cyclic voltam-metry technique in the absence and presence of 2- and 4-mercaptopyridine SAMs. The presence of these monolayers decreases the electrodeposition of copper to a great extent. This behaviour was rationalized to the very strong interactions between the gold electrode and the formed monolayer. This suggests that the formed monolayer is more stable than the Cu adlayer. 2MP monolayer shows a higher degree of inhibition of the electrodeposition of copper than 4MP. This stronger interaction is possibly due to the chelate structure of 2MP with the gold surface.

The influence of mercaptopyridine SAMs on gold electrode with an initially deposited copper has been also studied. Both 2MP and 4MP were found to displace the copper adlayer partially. This can be explained by the strength of interaction between the S-atom of the monolayer and the Au surface, which is greater than that between the Cu adatoms and the Au surface. 2MP can displace more copper adatoms than 4MP. This could be interpreted to the 2MP chelate structure while the structure of 4MP precludes the formation of a chelate with the Au surface, as in the case of 2MP. Thus, bonding to the surface is solely taking place through the sulfur atom. This may result in a diminution of the interaction of the adsorbed layer with the electrode so that 4MP displaces less copper. However, more copper is displaced by 4MP dissolved in water than in acidic solution. This can be explained due to the protonation of the N-atom in the "para" position of 4MP in acidic solution. Such protonation would cause (by inductive effect) a weakness of the S-metal bond. As a result, more Cu adatoms will be present on the Au surface.

The electron transfer of the redox couple is studied by cyclic voltammetry and electrochemical impedance techniques. The rate of electron transfer of the $Fe^{3+/2+}$ redox couple has been also investigated in the presence and absence of the monolayers. The charge transfer was suggested to occur through the defects (pinholes) that allow the electron transfer through the formed monolayers. Consequently the gold electrode modified with MPs can behave as a microarray electrode allowing molecules and ions from the electrolyte to reach the electrode surface. 2MP was found to retard the electron transfer reaction more than 4MP.

The surface enhanced Raman spectroscopy results are summarized and discussed. The formation of 2MP and 4MP monolayers on Au electrode is proved by the existence of Au-S stretching band which is located in the range of 215 to 250 cm^{-1} and at 263 cm^{-1} for 2MP and 4MP respectively. The experiments also suggest the perpendicular orientation of both 2MP and 4MP on the gold surface.

The EIM is also used to study the inhibition effect of the mercaptopyridine SAMs on the C60 steel electrode in 3.5% aqueous NaCl solution after 3 minutes immersion in aqueous solution of the mercaptopyridines. The polarization resistance and the inhibition efficiency are calculated. 2MP has more inhibition efficiency than 4MP.

Future work

The influence of 2-and 4-mercaptopyridines on the charge transfer process can be further investigated in neutral and basic solutions to give additional information about the mechanism of the charge transfer in different media and the effect of the media on the rate of the charge transfer.

The research can be continued to examine 2- and 4-mercaptopyridine monolayers as corrosion inhibitors as a function of different immersion time either in the inhibitor solution or in the probed electrolytic solution, various electrolytic media, a variety of temperature values, ect. The effect of these monolayers can be also investigated for different electrode materials.

2- and 4-mercaptopyridines self-assembled monolayers can be probed as a selective electrode to recognize selectively some metal ions, which are highly toxic to humans.

References

1   Franklin, B.; *Philos. Trans. R. Soc. London* **1774**, <u>64</u>, 445.

2   Pockels, A.; *Nature* **1891**, <u>43</u>, 437.

3   Pockels, A.; *Nature* **1892**, <u>46</u>, 418.

4   Pockels, A.; *Nature* **1893**, <u>48</u>, 152.

5   Pockels, A.; *Nature* **1894**, <u>50</u>, 223.

6   Rayleigh, L.; *Philos. Mag.* **1899**, <u>48</u>, 321.

7   Hardy, W. B.; *Proc. R. Soc. London A* **1912**, <u>86</u>, 610.

8   Devaux, H.; *Smithson. Inst. Ann. Rep.* **1913**, <u>261</u>.

9   Langmuir, I.; *J. Am. Chem. Soc.***1917**, <u>39</u>, 1848.

10   Langmuir, I.; *Trans. Faraday Soc.* **1920**, <u>15</u>, 62.

11   Blodgett, K.; *J. Am. Chem. Soc.* **1935**, <u>57</u>, 1007.

12   Blodgett, K.; *Phys. Rev.* **1937**, <u>51</u>, 964.

13   Schmidt, E.; Schurig, W.; Sellschopp, W. *Tech. Mech. Thermodyn.* **1930**, <u>1</u>, 53.

14   Nagle, W. M.; Drew, T. B.; *Trans. Am. Inst. Chem. Eng.* **1933**, <u>30</u>, 217.

15   Emmons, H.; *Trans. Am. Inst. Chem. Eng.* **1939**, <u>35</u>, 109.

16   Bigelow, W. C.; Pickett, D. L.; Zisman, W. A.; *J. Colloid Interface Sci.* **1946**, <u>1</u>, 513.

17   Blackman, L. C. F.; Dewar, M. J. S.; *J. Chem. Soc.* **1957**, 162, Part I – IV.

18   Schreiber, F.; *Progress in Surf. Sci.,* **2000,** <u>65</u>, 151.

19   Gaines Jr., G. L.; *Insoluble Monolayers at Liquid-Gas Interfaces*, Interscience, New York, **1966**.

20   Kaganer, V. M.; Möhwald, H.; Dutta, P.; *Rev. Mod. Phys.* **1999**, <u>71</u>, 779.

21   Ulman, A.; *An Introduction to Ultrathin Organic Films: From Langmuir-Blodgett to Self-Assembly*, Academic Press, Boston, **1991**.

22   Fendler, J.; *J. Mater. Sci.* **1987**, <u>30</u>, 323.

23   Tieke, B.; *Adv. Mater* **1990**, <u>2</u>, 222.

24   Tieke, B.; *Adv. Mater* **1991**, <u>3</u>, 532.

25   Swalen, J. D.; Allara D. L.; Andrade J. D.; Chandross E. A.; Garoff, S.; Israelachvili, J.; McCarthy T. J.; Murray, R.; Pease, R. F.; Rabolt, J. F.; Wynne K. J.; Yu H.; *Langmuir* **1987**, <u>3</u>, 932.

26   Zhang, Z. J.; Hou, S. F.; Zhu, Z. H.; Liu, Z. F.; *Langmuir* **2000**, <u>16</u>, 537.

27   Ulman, A.; *Chem. Rev.* **1996**, <u>96</u>, 1533.

28   Nuzzo, R. G.; Allara, D. L.; *J. Am. Chem. Soc.* **1983**, <u>105</u>, 4481.

29   Bain, C. D.; Troughton, E. B.; Tao, Y. T, Evall, J.; Whitesides, G. M., Nuzzo, R. G.; *J. Am. Chem. Soc.* **1989**, <u>111</u>, 321.

30   Laibinis, P. E.; Palmer, B. J.; Lee. S. W.; Jennings, G. K.; **1998** The synthesis of organothiols and their assembly into monolayers on gold. In: Ulman A (ed.) *Self-Assembled Monolayers of Thiols*, *Thin Films*. Vol. 24. Academic Press, San Diego, CA, pp. 1-41.

31   Porter, M. D.; Bright, T. B.; Allara, D. L.; Chidsey, C. E. D.; *J. Am. Chem. Soc.* **1987**, <u>109</u>, 3559.

32   Vericat, C.; Lenicov, F. R.; Tanco, S.; Andreasen, G.; Vela, M. E.; Salvarezza, R. C.; *J. Phys. Chem. B* **2002**, <u>106</u>, 9114.

33   Lin, S. Y.; Tsai, T. K.; Lin, C. M.; Chen, C. H.; *Langmuir* **2002**, <u>18</u>, 5473.

34   Kang, J. F.; Liao, S.; Jordan, R.; Ulman, A.; *J. Am. Chem. Soc.* **1998**, <u>120</u>, 9662.

35   Sun, L.; Crooks, R. M.; Ricoo, A. J.; *Langmuir* **1993**, <u>9</u>, 1775.

36   Bain, C. D.; Whitesides, G. M; *Adv. Mater.* **1989**, <u>1</u>, 506.

37   Folkers, J. P.; Zerkowski, J. A.; Laibinis, P. E.; Seto, C. T.; Whitesides, G. M.; *Supramolecular architecture*; Bein, T. Ed.; ACS Symposium Series 499; American Chemical Society: Washington, DC, **1992**; pp 10-23.

38   Lee, T. R.; Laibinis, P. E.; Folkers, J. P.; Whitesides, G. M; *Pure Appl. Chem.* **1991**, <u>63</u>, 821.

39   Whitesides, G. M.; Ferguson, G. S; *Chemtracts-Org. Chem.* **1988**, <u>1</u>, 171.

40   Beulen, M. W. J.; Kastenberg, M. I.; van Veggel, F. C. J. M.; Reinhoudt, D. N.; *Langmuir* **1998**, <u>14</u>, 7463.

41   Hubbard, A. T.; *Chem. Rev.* **1988**, <u>88</u>, 633.

42   Sun, L.; Johnson, B.; Wade, T.; Crooks, R. M.; *J. Phys. Chem.* **1990**, <u>94</u>, 8869.

43   Sabatani, E.; Cohen-Boulakia, J.; Breuning, M.; Rubinstein, I.; *Langmuir* **1993**, <u>9</u>, 2974.

44   Batz, V.; Schneeweiss, M. A.; Kramer, D.; Hagenström, H.; Kolb, D. M.; Mandler, D.; *J. Electroanal. Chem.* **2000**, <u>491</u>, 55.

45   Gölzhäuser, A.; Geyer, W.; Stadler, V.; Eck, W.; Grunze, M.; Edinger, K.; Weimann, T.; Hinze, P.; *J. Vac. Sci. Technol., B* **2000**, <u>18</u>, 3414.

46   Leung, T. Y. B.; Schwartz, P.; Scoles, G.; Schreiber, F.; Ulman, A.; *Surf. Sci.* **2000**, 458, 34.

47   Nielsen, J. U.; Esplandiu, M. J.; Kolb, D. M.; *Langmuir* **2001**, 17, 3454.

48   Baunach, T.; Kolb, D. M.; *Anal. Bioanal. Chem.* **2002**, 373, 743.

49   Gui, J. Y.; Lu, F.; Stern, D. A.; Hubbard, A. T.; *J. Electroanal. Chem.* **1990**, 292, 245.

50   Pettinger, B.; Mirwald, S.; Lipkowski, J.; *Ber. Bunsenges. Phys. Chem.* **1993**, 97, 395.

51   Sayre, C. N.; Collard, D. M.; *Langmuir* **1995**, 11, 302.

52   Willicut, R. J.; McCarley, R. L.; *Langmuir* **1995**, 11, 296.

53   Wurm, D. B.; Kim, Y.-T.; *Langmuir* **2000**, 16, 4533.

54   Alonso, C.; Pascual, M. J.; Salomón, A. B.; Abruña, H. D.; Gutierrez, A.; Ló-pez, M. F.; García-Alonso, M. C.; Escudero, M. L.; *J. Electroanal. Chem.* **1997**, 435, 241.

55   Hébert, P.; Le Rille, A.; Zheng, W. Q.; Tadjeddine, A.; *J. Electroanal. Chem.* **1998**, 447, 5.

56   Madueño, R.; Pineda, T.; Sevilla, J. M.; Blázquez, M.; *Langmuir* **2002**, 18, 3903.

57   Bryant, M. A.; Joa, S. L.; Pemberton, J. E.; *Langmuir* **1992**, 8, 753.

58   Armstrong, F. A.; Hill, H. A. O.; Walton, N. J.; *Acc. Chem. Res.* **1988**, 21, 407.

59   Cricenti, A.; Scarselli, M. A.; Paleari, R.; Mosca, A.; *J. Vac. Sci. Technol.* **1994**, 12B, 1494.

60   Mosca, A.; Paleari, R.; Arosio, P.; Cricenti, A.; Scarselli, M. A.; Generosi, R.; Selci, S.; Rovida, E.; *J. Vac. Sci. Technol.* **1994**, 12B, 1486.

61   Bron, M.; Holze, R.; *Electrochem. Soc.* 205th Meeting, Abs. 867.

62   Sawaguchi, T.; Mitzutani, F.; Yoshimoto, S.; Taniguchi, I.; *Electrochimica Acta* **2000**, 45, 2861.

63   Harford, S. T.; Taylor, D. L.; Abruña, H. D.; *J. Electrochem. Soc.* **1994**, 141, 3394.

64   Alonso, C.; Salomón, A. B.; Gutierrez, A.; López, M. F.; Escudero, M. L.; *Langmuir* **1999,** 15, 7014.

65   Taylor, D. L.; Abruña, H. D.; *J. Electrochem Soc.* **1993**, 140, 3402.

66   Alonso, C.; Pascual, M. J.; Abruña, H. D.; *Electrochimica Acta*, **1997**, 42, 1739.

67   Alonso, C.; López, M. F.; Gutiérrez, A.; Escudero, M. L.; *Surf. Interface Anal*. **2000**, 30, 359.

68   Zhang, H.; He, H. X.; Wang, J.; Liu, Z. F; *Langmuir* **2000**, 16, 4554.

69   Finklea, H.O.; Avery, S.; Lynch, M.; *Langmuir* **1987**, 3, 409.

70   Sellers, H.; Ulman, A.; Shnidman, Y.; Eilers, J. E.; *J. Am. Chem. Soc*. **1993**, 115, 9389.

71   Bain, C. D.; Evall, J.; Whitesides, G. M.; *J. Am. Chem. Soc*. **1989**, 111, 7155.

72   Rowe, G. K.; Creager, S. E.; *Langmuir* **1991**, 7, 2307.

73   Yang, Z.; Gonzalez-Cortes, A.; Jourquin, G.; Viré, J.; Kauffmann, J.; Delplancke, J.; *Biosens. Bioelectron*. **1995**, 10, 789.

74   Somorjai, G. A.; *Chemistry in Two Dimensions-Surfaces;* Cornell University Press: Ithaca, NY, **1982**.

75   Nuzzo, R. G.; Fusco, F. A.; Allara, D. L.; *J. Am. Chem. Soc.* **1987**, 109, 2358.

76   Strong, L.; Whitesides, G. M.; *Langmuir* **1988**, 4, 546.

77   Jin, Q.; Rodriguez, J. A.; Li, C. Z.; Darici, Y.; Tao, N. J.; *Surf. Sci*., **1999**, 425, 101

78   Finklea, H. O.; in: *Encyclopedia of Analytical Chemistry*, Ed. R. A. Meyers, John Wiley & Sons; Chichester, **2001**, Vol. 11, p. 10090.

79   Marotti, F.; Dissertation, Universitá "La Sapienza" di Roma, Italy, **2004**.

80   Hatchett, D. W.; Uibel, R. H.; Stevenson, K. J.; Harris, J. N.; White, H. S.; *J. Am. Chem. Soc.,* **1998,** 120, 1062.

81   Bishop, A. R.; Nuzzo, R.G.; *Current Opinion in Colloid and Interface* Science **1996**, 1, 127.

82   Dubois, L. H.; Nuzzo, R. G.; *Ann. Rev. Phys. Chem*. **1992**, 43, 437.

83   Kiryukhin, V.; Keimer, B.; Boltnev, R. E.; Khmelenko, V. V.; Gordon, E. B.; *Phys. Rev. Lett.* **1997**, 79, 1774.

84   Fung, A. S.; Kelley, M. J.; Koningsberger, D. C.; Gates, B. C.; *J. Am. Chem. Soc*. **1997**, 119, 5877.

85   Tao, Y. T.; Lin, W. L.; Hietpas, G. D.; Allara, D. L.; *J. Phys. Chem. B* **1997**, 101, 9732.

86   Alves, C. A.; Smith, E. L.; Porter, M. D.; *J. Am. Chem. Soc*. **1992**, 114, 1222.

87   Prime, K. L.; Whitesides, G. M. *Science* **1991**, 252, 64.

88   Murray, R. W.; *Molecular Design of Electrode Surface*; Techniques of Chemistry Series; John Wiley & Sons: New York, 1992; Vol. XXII.

89   Caldwell, W. B.; Campbell, D. J.; Chen, K.; Herr, B. R.; Mirkin, C. A.; Malik, A.; Durbin, M. K.; Dutta, P.; Huang, K. G.; *J. Am. Chem. Soc*. **1995**, 117, 6071.

90   Bahng, M. K.; Cho, N. J.; Park, J. S.; Kim, K. *Langmuir* **1999**, 14, 463.

91   Chidey, C. E. D.; *Science* **1991**, 251, 919.

92   Hickman, J. J.; Ofer, D.; Laibinis, P. E.; Whitesides, G. M.; *Science* **1991**, 252, 688.

93   Mirkin, C. A.; Ratner, M. A.; *Annu. Rev. Phys. Chem.* **1992**, 43, 719.

94   Li, D.; Ratner, M. A.; Marks, T. J.; Znang, C. H.; Yang, J.; Wong, G. K.; *J. Am. Chem. Soc.* **1990**, 112, 7389.

95   Wollman, E. W.; Kang, D.; Frisbie, C. D.; Larcovic, T. M.; Wrighton, M. S.; *J. Am. Chem. Soc.* **1994**, 116, 4395.

96   Tariov, M. J.; Burgess, D. R. F.; Gillen, G.; *J. Am. Chem. Soc.* **1993**, 115, 5305.

97   Kawanishi, Y.; Tamaki, T.; Sakuragi, M.; Seki, T.; Swuzki, Y.; Ichimura, K.; *Langmuir* **1992**, 8, 2601.

98   Smalley, J. F.; Feldberg, S. W.; Chidesey, C. E. D. et al.; *J. Phys. Chem.* **1995**, 99, 13141.

99   Baunach T.; Ivanova V.; Scherson D. A.; Kolb D. M.; *Langmuir* **2004**, 20, 2797.

100   Fawcett, W. R.; *J. Electroanal. Chem*. **1994**, 378, 117.

101   Collard, D. M.; Sayre, C. N.; *J. Electroanal. Chem*. **1994**, 375, 367.

102   Ohtsuka, T.; Sato, Y.; Uosaki, K.; *Langmuir* **1994**, 10, 3658.

103   Shimazu, K.; Yagi, I.; Sato, Y.; Uosaki, K.; *J. Electroanal. Chem*. **1994**, 372, 117.

104   Tang, X.; Schneider, T.; Buttry, D. A.; *Langmuir* **1994**, 10, 2235.

105   Abbot, N. L.; Gorman, C. B.; Whitesides, G. M.; *Lamgmuir* **1995**, 11, 16.

106   Wittstock, G.; Hesse, R.; Schuhmann, W.; *Electroanalysis* **1997**, 9, 746.

107   Tender, L. M.; Worley, R. L.; Fan, H.; Lopez, G. P.; *Langmuir* **1996**, 12, 5515.

108   Tender, L. M.; Opperman, K. A.; Hampton, P. D.; Lopez, G. P.; *Adv. Mater* **1998**, 10, 73.

109   Holze, R.; *Surf. Sci.* **1988**, 202, L612.

110   Bharathi, S.; Yegnaraman, V.; Prabhakara Rao, G.; *Langmuir* **1993**, 9, 1614.

111   Zhong, C. J.; Woods N. T.; Dawson G. B.; Porter M.; *Electrochem. Commun.* **1999**, 1, 17.

112   Lide D. R.; CRC Handbook of Chemistry and Physics. CRC Press: Boca Raton, FL, **1993**.

113   Laibinis, P. E.; Whitesides, G. M.; Allara, D. L.; Tao, Y.-T.; Parikh, A. N.; Nuzzo, R. G.; *J. Am. Chem. Soc.* **1991**, 113, 7152.

114   Ulman, A.; Eilers, J. E.; Tillman, N.; *Langmuir* **1989**, 5, 1147.

115   Nuzzo, R. G.; Dubois, L. H.; Allara, D. L.; *J. Am. Chem. Soc.* **1990**, 112, 558.

116   Chailapakul, O.; Sun, L.; Xu, C.; Crooks, R. M.; *J. Am. Chem. Soc.* **1993**, 115, 12459.

117   Reid, E. E.; *Organic Chemistry of biovalent sulfur*. Vol. III. Chemical Publ. Co., New York, 1996.pp.362-462.

118   Breiter, M. W; J. *Electrochem. Soc.* **1967**, 114, 1125.

119   Kolb, D. M.; Kotz, R.; *Surf. Sci.* **1977,** 64, 698.

120   Margheritis, D.; Salvarezza, R.C.; Giordano, M. C.; Arvia, A. J.; *J. Electro-anal. Chem.* **1987**, 229, 327.

121   Varga, K.; Zelenay, P.; Wieckowski, A.; *J. Electroanal. Chem.* **1992**, 330, 453.

122   McBreen, J.; O'Grady, W. E.; Tourillon, G.; Dartyge, E.; Fontaine, A.; *J. Electroanal. Chem.* **1991,** 307, 229.

123   White, J. H.; Abruña, H. D.; *J. Phys. Chem.* **1990,** 94, 894.

124   Wünsche, M.; Meyer, H.; Schumacher R.; *Electrochim. Acta* **1995,** 40, 629.

125   Chaki, N.K.; Aslam, M.; Sharma, J.; Vijayamohanan, K.; *Proc. Indian Acad. Sci.* **2001**, 113, 659.

126   Finklea, H.O.; Snider, D.A.; Fedyk, J.; Sabatani, E.; Gafni Y.; Rubinstein, I.; *Langmuir*, **1993**, 9, 3660.

127   Sabatani, E.; Rubinstein, I.; *J. Phys. Chem.*, **1987**, 91, 6663.

128   Sabatani, E.; Rubinstein, I.; *J. Electroanal. Chem*. **1987**, 219, 365.

129   Rubinstein, I.; Steinberg, S.; Tor, Y.; Shanzer A.; Sagiv, J.; *Nature*, **1988**, 332, 426.

130   Bard, A.J.; Faulkner, L.R.; *Electrochemical Methods, Fundamentals and Applications*, Wiley, New York, **2000.**

131   Astier, Y.; Bond, A.; Wijma, H.; Canters, G.W; Hill, H.; Davis, J. J.; *Electroanalysis*, **2004**, <u>16</u>, 1155.

132   Wang, J.; Zeng, B. H.; Fang, C.; Zhou, X.Y.; *Anal. Sci.* **2000**, <u>16</u>, 457.

133   Campuzano, S.; Pedrero, M.; Montemayor, C.; Fatás, E.; Pingarrón, J.M.; *J. Electroanalytical Chemistry*, **2006**, <u>586</u>, 112.

134   de Sousa, J. R.; Parente, M. M. V.; DiÓgenes, I. C. N.; Lopes, L. G. F.; Neto, P.; Temperini, M. L. A.; Batista, A. A.; Moreira, Í.; *J. Electroanalytical Chemistry*, **2004**, <u>566</u>, 443.

135   Diao, P.; Guo, M.; Jiang, D.; Jia, Z.; Cui, X.; Gu, D.; Tong, R.; Zhong, B.; *J. Electroanal. Chem.* **2000**, <u>480</u>, 59.

136   Diao, P.; Jiang, D.; Cui, X.; Gu, D.; Tong, R.; Zhong, B.; *J. Electroanal. Chem.* **1999**, <u>464</u>, 61.

137   Bandyopadhyay, K.; Vijayamohanan, K.; Shekhawat, G. S.; Gupta, R. P.; *J. Electroanal. Chem.* **1998**, <u>447</u>, 11.

138   Bandyopadhyay, K.; Vijayamohanan*,* K.; Venkataramanan, M.; Pradeep, T.; *Langmuir* **1999,** <u>15</u>*,* 5314.

139   Sur, U. K.; Lakshminarayanan, V.; *J. Electroanal. Chem.* **2001**, <u>516</u> , 31.

140   Jun, Y. Y.; Beng, K. S.; *Electrochem. Comm.* **2004***,* <u>6</u>, 87.

141   Berchmans, S.; Yegnaraman, V.; Rao, G.P.; *J. Sol. State Electrochem.*, **1998**, <u>3</u> , 52.

142   Protsailo, L.V.; Fawcett, W. R.; *Electrochim. Acta* **2000**, <u>45</u>, 3497.

143   Mendes, R. K.; Freire, R. S.; Fonseca, C. P.; Neves, S.; Kubota, L. T.; *J. Braz. Chem. Soc.,* **2004**, <u>15</u>, 849.

144   Janek, R. P.; Fawcett, W. R.; Ulman, A.; *Langmuir* **1998**, <u>14</u>, 3011.

145   Bandyopadhyay, K.; Patil, V.; Sastry, M.; Vijayamohanan, K.; *Langmuir* **1998**, <u>14</u>, 3808.

146   Sluyters-Rehhach, M.; Sluyters J. H.; "*Electroanalytical Chemistry*", ed. A. J. Bard, 1970, Vol. 4, Marcel Dekker, New York.

147   Boubour, E.; Lennox, B.; *Langmuir* **2000**, <u>16</u>, 4222.

148   Barsonkov, E.; Macdonald, J. R.; *Impedance Spectroscopy: Theory, Experimental and applications*, 2nd ed., Wiley-Interscience, New York (**2005**).

149   Pessôa, M. M. B.; Temperini, M. L. A.; *J. Raman Spectrosc.* **2002**, <u>33</u> 50.

150   Zheng, J.; Zhou, Y.; Li, X.; Ji, Y.; Lu, T.; Gu, R.; *Langmuir* **2003,** <u>19</u>**,** 632.

151 Enlow, P. D.; Buncick, M.; Warmack, R. J.; Vo-Dinh, T.; *Anal. Chem.* **1988,** 58**,** 1119.

152 Otto, C.; de Mul, F. F. M.; Huizinga, A.; Greve, J.; *J. Phys. Chem.* **1988**, 92**,** 1239.

153 Ooka, A. A.; Garrell, R. L.; *Biopolymers (Biospectroscopy)* **2000**, 57**,** 92.

154 Jang, N. H.; *Bull. Korean Chem. Soc.* **2002**, 23, 1790.

155 Bjerneld, E. J.; Fölldes-Papp, Z.; Käll, M.; Rigler, R.; *J. Phys. Chem. B*, **2002**, 106, 1213.

156 Kneipp, K.; Wang, Y.; Kneipp, H.; Perelman, L. T.; Itzkan, I.; R. R. Dasari, R. R.; Feld, M. S.; *Phys. Rev. Lett.* **1997**, 78, 1667.

157 Bryant, M. A.; Pemberton, J. E.; *J. Am. Chem. Soc.* **1991**, 113, 3629.

158 Bryant, M. A.; Pemberton, J. E.; *J. Am. Chem. Soc.* **1991**, 113, 8284.

159 Herzberg, G.; *Infrared and Raman Spectra of Polyatomic Molecules*; Van Nostrand Reinhold: New York, **1945**; pp 534-537.

160 Dunbar, T. D.; Cygan, M. T.; Bumm, L. A.; McCarty, G. S.; Burgin, T. P.; Reinerth, W. A.; Jones, L.; Jackiw, J. J.; Tour, J. M.; Weiss, P. S.; Allara, D. L.; *J. Phys. Chem. B* **2000**, 104, 4880.

161 Chang, R. K. *Ber. Bunsen-Ges. Phys. Chem.* **1987**, 91, 296.

162 Baldwin, J. A.; Blanka Vlčková, B.; Andrews, M. P.; Ian S. Butler, I. S.; *Langmuir* **1997,** 13, 3744.

163 Baldwin, J; Schühler, N.; Butler, I. S.; Andrews, M. P.; *Langmuir* **1996,** 12, 6389.

164 Spinner, E.; *J. Chem. Soc.*, **1960**, 1237.

165 Green, J. H. S.; Kynaston, W.; Paisley, H. M. *Spectrochim. Acta* **1963**, 19, 549.

166 Spinner, E. *J. Chem. Soc.* **1963**, 3860.

167 Joo, H. T.; Kim, M. S.; Kim, K.; *J. Raman Spectrosc.* **1987**, 18, 57.

168 Dollish, F. R.; Fateley, W. G.; Bentley, F. F. *CharacteristicRaman Frequencies of Organic Compounds*; John Wiley & Sons: New York,1974.

169 Taniguichi, I.; Iseki, M.; Yamaguchi, H.; Yasukouchi, K.; *J. Electroanal. Chem.* **1985**, 186, 299.

170 Stekas, T.; Diamandopoulos, P.; *J. Phys. Chem.* **1990**, 94, 1986.

171 Hu, J.; Zhao, B.; Xu, W.; Li, B.; Fan, Y.; *Spectrochimica Acta* **2002**, 58A 2827.

172   Albert, A.; Barlin, G. B.; *J. Chem. Soc.* **1959**, 2384.

173   Joo, S. W.; Han, S. W.; Kim, K.; *J. Phys. Chem.* **2000,** 104B, 6218.

174   Szafranski, C. A.; Tanner, W.; Laibinis, P. E.; Garrell, R. L.; *Langmuir* **1998**, 14, 3570.

175   Joo, S. W.; Han, S. W.; Kim, K.; *Appl. Spectrosc.* **2000**, 54, 378.

176   Carron, K.; Hurley, L. G.; *J. Phys*. *Chem*. **1991**, 95, 9979.

177   Akyuz, S.; Dempster, B.; Morehouse, R. L.; Suzuchi, S. *J. Mol. Struct*. **1973**, 17, 105.

178   Colthrup, N. B.; Daly, L. H.; Wiberly, S. E.; Fateley, W. G.; Grasselli, J. G. *Handbook of Characteristic Infrared and Raman Frequencies of Inorganic Compounds*; Academic Press: New York, **1991**.

179   Joo, T. H.; Yim, Y. H.; Kim, K.; Kim, M. S.; *J. Phys*. *Chem*. **1989**, 93, 1422.

180   Yu, H.; Xia, N.; Liu, Z.; *Anal. Chem.* **1999**, 71, 1354.

181   Jung, H.S.; Kim, K.; Kim, M. S.; *J. Mol. Struct*. **1997**, 407, 139.

182   Moscovits, M.; Shu, S.; *J. Phys*. *Chem*. **1984**, 88, 5526.

183   Creighton, J. A.; *Surf. Sci.* **1985**, 158, 211.

184   Creighton, J. A.; *Surf. Sci.* **1983**, 124, 211.

185   Vlcková, B.; Barnett, S. M.; Kanigan, T.; Butler, I. S.; *Langmuir* **1993**, 9, 3234.

186   Lautie, A.; Hervieu, J.; Beloc, J.; *Spectrochim. Acta* **1983**, 39A, 367.

187   Zhang, H.; Evans, S. D.; Henderson, J. R.; Miles, R. E.; Shen, T.; *J. Phys. Chem. B* 2003, 107, 6087.

188   Shunmugam, R.; Sathyanarayana, D. N.; *Spectrochim. Acta* **1984**, 40A, 757.

189   Stoyanov, S.; Petkov, I.; Antonov, L.; Stoyanova, T.; Karagiannidis, P.; Aslanidis, P.; *Can. J. Chem.* **1990**, 68, 1482.

190   Pang, Y. S.; Hwang, H. J.; Kim, M. S.; *Journal of Molecular Structure*, **1998**, 441, 63.

191   Zanneti, R.; *Chem. Eng. (NY)* **1990**, 97, 5.

192   Trabanelli, G.; *Corrosion* **1991,** 47, 410

193   Samide, A.; Bibicu, I.; Rogalski, M.; Preda, M.; *Acta Chim. Slov.* **2004**, 51, 127.

194   Cabrera-Sierra, R.; Garcia, I.; Sosa, E.; Oropeza, T.; Gonzalez, I.; *Electrochim. Acta* **2000**, 46, 487.

195   Altoe, P.; Pimenta, G.; Moulin, C. F.; Diaz, S. L.; Mattos, O. R.; *Electrochim. Acta* **1996**, 41, 1165

196   Roberge, P. R.; Sastri, V. S.; *Corrosion Science* **1993**, 35, 1503.

197   Garveric, L.; (Ed.), *Corrosion in the petrochemical Industry*. ASM International, USA 1995.

198   Matsunami, K.; Kato, T.; Sugimoto, K.; *IJPVP* **1991**, 45, 179.

199   Tan, Y. J.; Bailey, S.; Kinsella, B.; *Corrosion Science* **1996**, 38, 1545.

200   Monticelli, C.; Frignani, A.; Trabanelli, G.; *Cement and Concrete Research* **2000**, 30, 635.

201   El Achouri, M.; Infante, M. R.; Izquierdo, F.; Kertit, S.; Gouttaya, H. M.; Nciri, B.; *Corrosion Science* **2001**, 43, 19.

202   Ashassi-Sorkhabi, H.; Nabavi-Amri, S. A.; *Acta Chim. Slov.* **2000**, 47, 507.

203   Ashassi-Sorkhabi, H.; Nabavi-Amri, S. A.; *Acta Chim. Slov.* **2002**, 44, 2239.

204   Bastidas, J. M.; Polo, J. L.; Torres, C. L.; Cano, E.; *Corrosion Science* **2001**, 43, 269.

205   Orazem, M. E.; Agarwal, P.; Garcia-Rubio, L. H.; *Materials Science Forum* **1995**, 192–194, 563–572.

206   Bonora, P. L.; Deflorian, F.; Fedrizzi, L.; *Electrochimica Acta* **1996**, 41, 1073.

207   Uhlig, H. H.; Revie, R. W. *Corrosion and Corrosion Control*, 3rd ed.; John Wiley and Sons: New York, 1985.

208   Vastag, Gy.; Szöcs, E.; Shaban, A.; Kálmán, S.; *Pure Appl. Chem.*, **2001**, 73, 1861.

Publication

- Effect of temperature on dissolution of aluminium in acid containing organic compounds. Ibrahim Z. Selim; Amal A. Khedr; **Nazly A. Ibrahim**, Bulletin of Electrochemistry **16** (2000) 186.

Selbständigkeitserklärung

Hiermit erkläre ich an Eides statt, die vorliegende Arbeit selbständig und ohne unerlaubte Hilfsmittel durchgeführt zu haben.

Nazly Abd el-salam Ibrahim Hassan

Nationality: Egyptian

Date and Place of Birth: 12.03.1968 in Egypt

Education

1982-1985	High secondary school, Scientific Stream, Taha Husien S.S.G, Egypt
1985-1989	Alexandria University, Egypt, Bachelor Degree of Science (chemistry, very good rating).
1994	Cairo University, Egypt, Post graduate studies, Inorganic chemistry department.
1994-1997	Cairo university, Egypt, Master of Science (inorganic and physical chemistry), Master Thesis: supervisors Prof. Dr. Amal Abu-bakr Khedr, Prof. Dr. Afaf El-Said Mahgoub, Prof. Dr. Ibrahim Selim, Title of Master Thesis "Evaluation of some chalcones derivatives as corrosion inhibitors for aluminum in hydrochloric acid solution".
2002-2007	Ph. D. student, Chemnitz University of Technology, supervisor Prof. Dr. Rudolf Holze.

Professional Experience

1991-1997	Assistant Researcher**,** Physical Chemistry Department, National Research Center, Cairo, Egypt.
1997-	Researcher Assistant**,** Physical Chemistry Department, National Research Center, Egypt.
2000-2001	Assistant Researcher**,** Physical Chemistry Department, Hamburg University, Germany.
2001-2005	Assistant Researcher**,** Physical Chemistry Department, Chemnitz University of Technology, Germany.